



OPEN ACCESS

EDITED BY

Yongqiang Zhou,
Chinese Academy of Sciences (CAS), China

REVIEWED BY

Shankai Zhang,
Huaiyin Normal University, China
Erdi Abi,
Chongqing Jiaotong University, China

*CORRESPONDENCE

Tingchun Li

✉ tchli_sd@163.com

RECEIVED 10 June 2023

ACCEPTED 23 August 2023

PUBLISHED 11 September 2023

CITATION

Zhu Q, Li T, Lou Q, Liu Y, Li C
and Chen J (2023) Stability mechanisms
of soft rock mining roadways through
roof cutting and pressure relief: an
exploratory model experiment.
Front. Ecol. Evol. 11:1237894.
doi: 10.3389/fevo.2023.1237894

COPYRIGHT

© 2023 Zhu, Li, Lou, Liu, Li and Chen. This is
an open-access article distributed under the
terms of the [Creative Commons Attribution
License \(CC BY\)](https://creativecommons.org/licenses/by/4.0/). The use, distribution or
reproduction in other forums is permitted,
provided the original author(s) and the
copyright owner(s) are credited and that
the original publication in this journal is
cited, in accordance with accepted
academic practice. No use, distribution or
reproduction is permitted which does not
comply with these terms.

Stability mechanisms of soft rock mining roadways through roof cutting and pressure relief: an exploratory model experiment

Qingwen Zhu¹, Tingchun Li^{1*}, Qingnan Lou², Yishuai Liu³,
Chunping Li⁴ and Jiangang Chen⁴

¹Shandong Key Laboratory of Civil Engineering Disaster Prevention and Mitigation, Shandong University of Science and Technology, Qingdao, China, ²School of Earth Sciences and Engineering, Nanjing University, Nanjing, China, ³College of Pipeline and Civil Engineering, China University of Petroleum (Huadong), Qingdao, China, ⁴Inner Mongolia Shanghaimiao Mining Co., Ltd., Ordos, China

Introduction: Soft rock mining roadways are severely deformed and damaged during coal mining. Blindly increasing the support strength not only has little effect but also wastes material resources.

Methods: Maintaining the original support parameters, model experiments were conducted to investigate the mechanism of pressure relief protection of the front soft rock mining roadway by cutting the roof behind the longwall face. The roof-cutting height was 2.5 times the coal thickness, the angle was 10°, and the advance distance is 0.

Results: The study found that the abutment stress borne by the roof of the original roadway was transferred to the coal seams to be mined. The average stress of the coal seams increased by 10%, while the average stress of the surrounding rock in the front roadway decreased by 12.57%. The roof cutting weakened the influence of the overlying strata in the gob on the rear roadway. The stability of the rear roadway also weakened the traction effect on the front roadway. The vertical convergence of the front roadway decreased by 27.3%, and the deformation of the coal pillars decreased by 15.7%.

Discussion: The roof cutting reduced the stress of the front roadway to the peak failure stress, fundamentally weakening the main factor that induced the deformation of the front roadway. Numerical simulations were performed to research the deformation and stress distribution properties of the surrounding rock after roof cutting, and the model experimental results were validated. Finally, engineering recommendations are presented, which are expected to provide a reference for controlling the roadway stability of soft rock masses.

KEYWORDS

soft rock mining roadway, model experiment, large deformation, failure characteristics, roof cutting and pressure relief, roadway protection

1 Introduction

Increased demand for coal, which accounts for a large proportion of China's energy production and consumption (Lv et al., 2021), has led to a shift of mining centers to the west of China (Zhang et al., 2021). Some areas of western China host soft rock (e.g., Jurassic rocks), resulting in the weak bearing and poor cementation of surrounding rocks in engineering projects. This is especially true in the mudstone and sandy mudstone strata in the Jurassic System. Under these conditions, there have been many difficulties with the support of roadways, resulting in soaring costs and delays in construction (Arora et al., 2021). Many scholars have analyzed the deformation trends of soft rock roadways (Table 1). Research has shown that roadways within the mining stress advanced range of influence can be severely damaged (Mo et al., 2020). This not only affects mining progress but also poses a safety hazard. As a result, reducing the deformation and weakening the failure of mining roadways in soft rock strata has become an urgent problem to be addressed.

In terms of the failure mechanism of soft rock mining roadways, Xu et al. (2021) studied the bidirectional asymmetric failure mode of soft rock roadways in fully mechanized top coal caving mining and summarized the main reasons for the failure. Zhu et al. (2022a) summarized three typical stages of deformation in typical roadways and studied the characteristics of surrounding rock failure. Yang et al. (2017) studied the failure process of soft rock roadways under different support factors and explored the deformation and crack evolution laws of the surrounding rock. Uneven stress and weak surrounding rock are internal factors of failure, while unreasonable support is an external factor of this effect (Zhan et al., 2020). A summary of the failure factors provides an important reference for control measures in soft rock roadways.

In terms of support techniques for soft rock mining roadways, Shen (2014) studied the invalidation features of soft-strata-mining roadways in longwall panels, optimized the bolt (cable) arrangement and increased the pretightening force. Pan et al. (2017) researched the effect of the water-cement ratio on the grout reinforcement effect of mining roadways. Wang et al. (2021) studied the instability mechanism of typical soft rock strata roadways in the Puhe Coal Mine and optimized the reinforcement scheme of "bolt-cable mesh-shotcrete". Zhu et al. (2023) studied the characteristics of roadway failure in Jurassic soft rock and proposed countermeasures, such as fiber shotcrete, increasing the length and prestress of the cables. Hao et al. (2021) analyzed the main cause of the deformation of mining roadways and proposed an active-passive coupling support scheme. Tian et al. (2022) created a reinforcement scheme of "bolt-cable-shotcrete + deep and shallow hole grouting" according to the support practice of the Wangjialing Coal Mine. The above studies proposed targeted support schemes for mining roadways under various soft rock conditions and achieved good results. Some new support components and ideas for the yieldable support of soft-rock tunnels were also introduced for roadways (Öge, 2021). However, the improvement measures did not break away from traditional thinking and mainly involved strengthening support (Figure 1A), e.g., grouting, high-strength bolts, energy-absorbing cables, arch frames, combined support, and narrowing spacing (Li et al., 2022a). This means a higher cost and longer construction period, but it still fails to change the current situation of soft-rock roadway deformation and failure.

It has been determined that stress is an important cause of roadway failure (Mishra et al., 2021). If the stress can be mitigated, then the load on the roadway can be substantially reduced. The idea of roof cutting and pressure relief (RCPR) from Professor He's team

TABLE 1 Comparison of research status and technical solutions.

Research object	Research contents	Technology or support scheme	Author
Soft rock roadway	Roadway failure mechanism	Grouting, high pretensioning	Shen (2014)
Deep coal roadway	Bolt-grouting support parameters	Bolt-grouting support	Pan et al. (2017)
Deep soft rock roadway	Large deformation and failure mechanism	Bolt-cable-mesh-shotcrete + shell	Yang et al. (2017)
Mining roadway	Large deformation of broken soft coal	Bolt, W steel belt + cable, cable beam	Hao et al. (2021)
Soft rock roadway	Roadway deformation and instability mechanism	Bolt + anchor cable net + concrete shotcrete	Wang et al. (2021)
Gob side coal roadway	Asymmetric deformation mechanism and control	Strengthening support of weak structure	Xu et al. (2021)
Mining roadway	Asymmetric deformation failure mechanism	Bolt-cable-shotcrete, grouting	Tian et al. (2022)
Deep soft rock roadway	Failure and stability analysis	Bolt-mesh-shotcrete	Zhu et al. (2022a)
Soft mining roadway	Deformation and failure mechanism	Bolt-mesh-cable-shotcrete	Zhu et al. (2023)
Mining roadway	Influenced factors of roadway deformation	Pressure relief by roof cutting	Yang et al. (2019)
Gob side entry retention	Fracturing mechanisms, deformation characteristics	Advance prefabricating, cables + hydraulic props, beams, U steel	Guo et al. (2021)
No-pillar roadway	Roof cutting distance, roof failure limit	Advance roof-cutting, cables + hydraulic props, beam	Lou et al. (2021)
Gob side entry retaining	Deformation mechanism and control technology	Advance roof presplitting, combined support	He et al. (2022)
Deep mine hard roof	Roadway stability, stress relief technique	Advance roof cutting, strengthening support	Sun et al. (2022)
Deep mining roadway	Roof-cutting and energy-absorbing mechanism	Advance roof-cutting, strength energy combined support	Wang et al. (2022a)

has provided a new perspective of roadway stability (Figure 1B). RCPR technology has become a research focus in recent years. Sun et al. (2022) studied the parameters of roof cutting and analyzed the influence of pressure relief technology on hard rock roofs. He et al. (2022) studied the surrounding rock movement pattern of gob-side entry retaining (GSER) with RCPR. Wang et al. (2022a) proposed a roof-cutting energy-absorbing support scheme for the problem of the failure of coal mining roadways. Guo et al. (2021) investigated the roof rupture mechanism of the GSER, proposed a new support scheme, and verified it on site. Lou et al. (2021) found that controlling the roof-cutting distance can diminish roadway deformation. Yang et al. (2019) improved the stress environment of the roadway and controlled the deformation of adjacent roadways by presplitting blasting. Research and practice by the aforementioned scholars have shown that the key to GSER with RCPR is “advance roof cutting + strengthened support” (Table 1). Advanced roof cutting can prevent the integrity of the remaining roadway roof from being damaged by mining stress. At the same time, it also maintains a certain distance between roof-cutting operations and the longwall mining face without affecting the coal mining progress. While advanced roof cutting can prevent

mechanical connections between roof rock layers in advance, the roadway after roof cutting must adopt strengthened support to control deformation (Figure 1B).

The engineering context of this paper is typical of soft rock, in which coal pillars are retained for mining. If the technical scheme of GSER is replicated, the support strength and cost will be further increased. To achieve the goal of improving the stability of coal mining roadways at the lowest cost, advanced roof-cutting schemes in soft rock are not recommended. Based on the reality that increasing support has failed to improve the deformation and damage of soft rock roadways, roof cutting technology is applied to the protection of mining roadways. A soft rock roadway retains its original support, and the progress of the roof cutting and the mining advance of the panels are consistent (Figure 1C). To manage the roof collapse of the gob with roof cutting can be difficult; currently, there is limited research on this technique, and the mechanism is poorly understood.

Thus, the fundamental parameters of roof cutting are determined in this work by theoretical calculations for model experiments. For the model experiment, difficulties such as similar roadway support structures, similar gobs, simulated

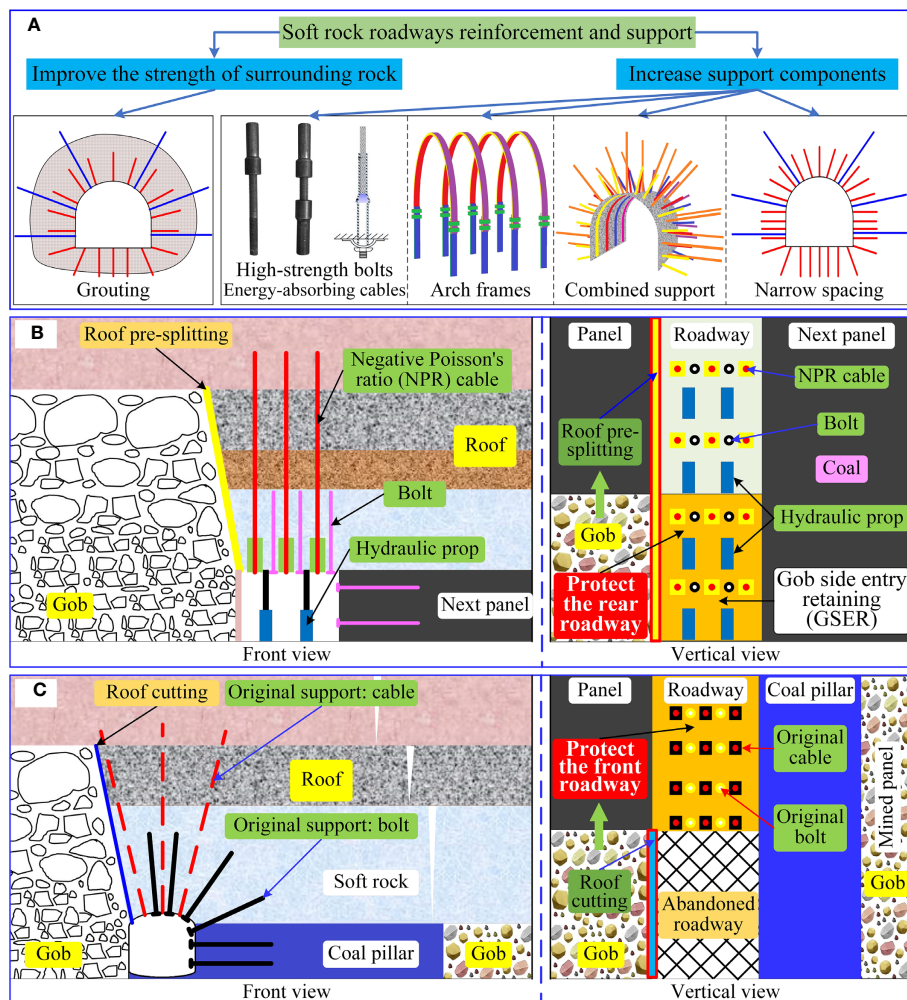


FIGURE 1 Methods for improving the stability of roadways. (A) Adding support. (B) RCPR with GSER. (C) Roof cutting to protect the front roadway.

mining and roof cutting devices are overcome. The traditional test process is innovated, and two true triaxial model experiments are carried out. This paper analyzes the influence of the stress and deformation in front of the mining roadway under the action of roof cutting of the roadway. Through two comparative model experiments, the mechanism of RCPR for roadway protection in soft rock is revealed. Finally, we present numerical simulations and optimization measures to validate the model test conclusions. It is expected that this work will provide a reference for roadways under similar geological conditions.

2 Engineering overview

The Xinshanghai No. 1 Coal Mine is situated in Shanghaimiao town, Ordos city, China, and currently produces No. 15 coal from the Yan'an Formation. The average thickness of the No. 15 coal in the 114156 panel is 4.0 m, and the average inclination angle is 6°.

The right side of the 114156 panel is a coal pillar and is called the 114152 gob. The roadway is supported by a “bolt-cable mesh-shotcrete + steel belt”. In addition, the floor was resprayed with 300 mm-thick concrete using an inverted arch structure. The roadway uses high-strength prestressed bolts (Figure 2A). The on-site vertical stress of the roadway is 8.5 MPa, and the horizontal stresses are 11.2 MPa and 14.11 MPa.

The support was still unable to resist the deformation of the roadway, and the roadway was severely damaged in advance during coal mining. The damage characteristics are roof subsidence, steel belt failure, sidewall bulging and severe floor heaving. To resume production, the damaged roadway had to be repaired and reinforced. After a period of repair, the roadway was still damaged, and the soft rock mining roadway fell into a vicious cycle of “repair–destruction–repair–redestruction”. The roof and floor of the No. 15 coal seam are composed of mudstone and sandy mudstone, respectively. X-ray diffraction analysis was conducted on the mudstone and sandy mudstone (Table 2). The kaolinite and illite

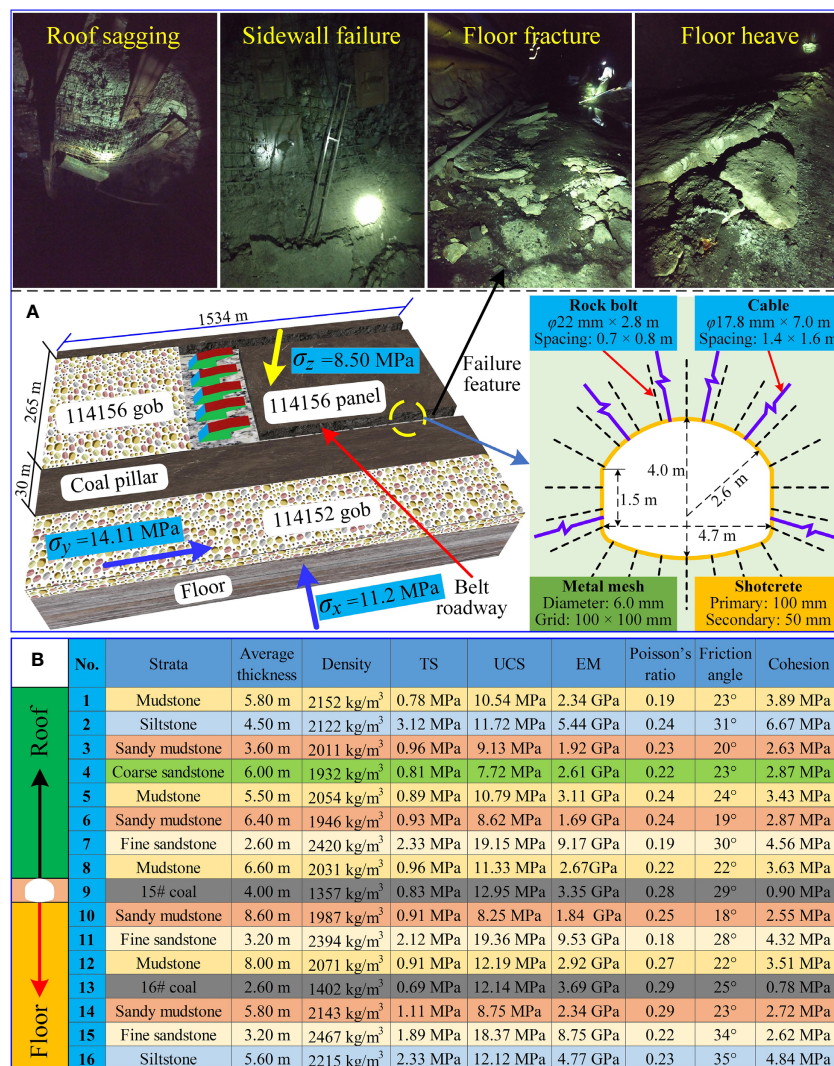


FIGURE 2 Overview of the engineering background. (A) Panel and belt roadway. (B) Formation lithology and physical parameters.

in the internal components of the mudstone and sandy mudstone together determine the mechanical properties of the rocks. Therefore, they are soft rocks with poor cementation (Zhou et al., 2014). The mechanical properties of the main rock strata are obtained through rock mechanics experiments (Figure 2B).

3 Geomechanical model experiments

3.1 The basic principles of RCPR and model experimental design

To date, the technology of RCPR is relatively mature. To protect the stability of the GSER behind the longwall face, it is necessary to cut the roof a certain distance ahead of the longwall face when adopting RCPR technology. As advanced roof cutting weakens the integrity of the bearing structure of the roadway roof, negative Poisson’s ratio (NPR) cables, high-strength bolts and hydraulic props are often used for high-strength support of the GSER. High-strength supports form a cantilever-beam composite structure in the roof to control the deformation of the surrounding rock, and the remaining roadway can serve the next panel (Bian et al., 2022). The oriented blasting cuts the roof rock layer to a certain height in a directional manner, blocking the stress transfer between the roadway roof and the gob roof. The cracks formed within the roof contribute to the directional collapse of the roof, which not only reduces the value of the advanced abutment stress but also weakens the deformation of the mining roadway. The collapsed gangue supports the overlying strata of the gob, reducing the intensity of the abutment stress. The idea of “GSER for RCPR” is used to protect the stability of soft rock mining roadways.

However, there are significant differences in the rock characteristics, strata thickness, and mining methods of each roadway, making it impossible to replicate existing experience. Especially under soft rock conditions, the parameters of roof cutting are still unclear, and hasty field tests can not only affect the progress of coal mining but also aggravate roadway deformation. Based on the existing results, the basic parameters of roof cutting are calculated (Figure 3A). Analyzing the force and sliding properties of the fracture block and calculating the selection range of the cutting angle suggests (Chen et al., 2019; Zhang et al., 2022):

$$\theta \geq \varphi' - \arctan(2(h_m - \omega)/L) \tag{1}$$

θ is the roof cutting angle, °. φ' is the residual friction angle of the rock, 22-32°. h_m is the thickness of the main roof, 2.6 m. L is the average fracture length of the main roof, 15 m. ω is the subsidence of rock blocks, 0.7 m. Thus, it is calculated that $\theta \geq 7.78-17.78^\circ$. The roof-cutting angle selected for the model experiment is 10°.

The roof-cutting height should ensure that the collapsed gangue fills the entire gob and provides support for the gob roof. However, the cost of drilling and explosives must not be wasted. The height of the roof cutting is calculated as follows (He et al., 2019):

$$H_p = (H_M - \Delta H_1 - \Delta H_2)/(K - 1) \tag{2}$$

H_p is the roof-cutting height, m; H_M is the height of mining, 4.0 m; ΔH_1 is the settlement of the gob roof, m; ΔH_2 is the gob floor heave, m; K is the rock bulking factor. The thicknesses of the roof mudstone and fine sandstone are calculated by weighting them and taking the average value $K=1.4$. Without considering the deformation of the gob ($\Delta H_1=0, \Delta H_2=0$), the calculated cutting height is 10.0 m.

If the roof rock layer is equivalent to a beam structure, it is called a “rock beam”. Before roof cutting, the “rock beam” is a fixed support structure, while after roof cutting, the “rock beam” is a simple support structure (Figure 3B). Roof cutting can effectively increase the deformation of the “rock beam” in the gob, transform the fixed structure into a rotatable structure, and ensure its smooth collapse (Sun et al., 2022). Under the action of mining stress, the roadway in front of the longwall face is greatly deformed and destroyed. If the roof is presplit, then it accelerates the destruction of the roof of the soft-rock roadway. The progress of coal mining and roof cutting needs to be consistent, and the roof cutting distance in front of the longwall mining face is 0.

Based on the current deformation status of soft rock mining roadways, the deformation patterns of the roadways were studied through a model experiment (Model A) and numerical simulations. To validate the roof-cutting effect, a comparative model experiment (Model B) was planned. The only difference between the two model experiments is that Model B cuts the roadway roof (Figure 4). The roof-cutting angle and depth are 10° and 10 m, respectively. The geometrically similar scale was determined by combining the site conditions, test devices and boundary conditions (Halder and Manna, 2021).

TABLE 2 Mineral composition analysis.

Rock strata	Sample	Quartz	Kaolinite	Octahedrite	Illite	Microcline
Mudstone	NY-D-1	10.8%	33.4%	24.1%	18.8%	12.9%
	NY-D-2	11.2%	34.1%	23.9%	19.2%	11.6%
	NY-D-3	10.7%	33.5%	24.4%	17.4%	14.0%
	NY-D-4	11.0%	33.8%	24.1%	18.4%	12.7%
Sandy mudstone	SNY-D-1	33.8%	18.7%	20.5%	27.0%	0
	SNY-D-2	35.7%	19.2%	21.1%	24.0%	0
	SNY-D-3	36.8%	18.4%	20.4%	24.4%	0
	SNY-D-4	32.1%	18.8%	20.8%	28.3%	0

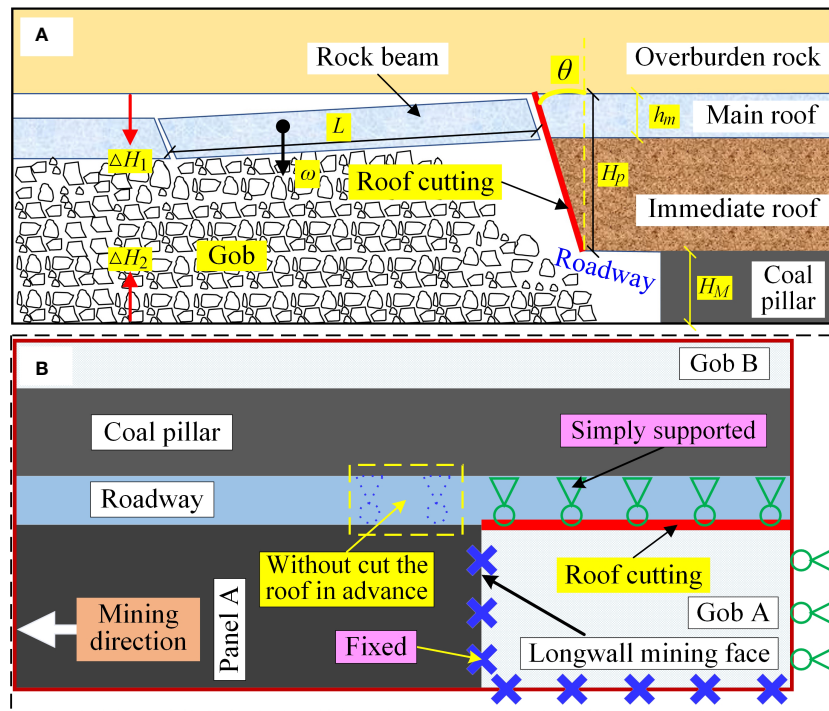


FIGURE 3 Movement and boundary conditions of the gob roof. (A) Movement of rock strata after roof cutting. (B) Boundary conditions of the rock beam.

3.2 Similar materials and similar principles

$$C_i = i_p / i_M \quad (3)$$

The model test needs to abide by the similarity principles, and the ratios of the physical parameters of the physical model and the on-site prototype are similar (Ghabraie et al., 2015). Definition:

C_i is the similarity scale of a certain parameter, i_p is the prototype parameter, and i_M is the model parameter. The model and prototype satisfy the three equations in the theory of mechanics: the balance

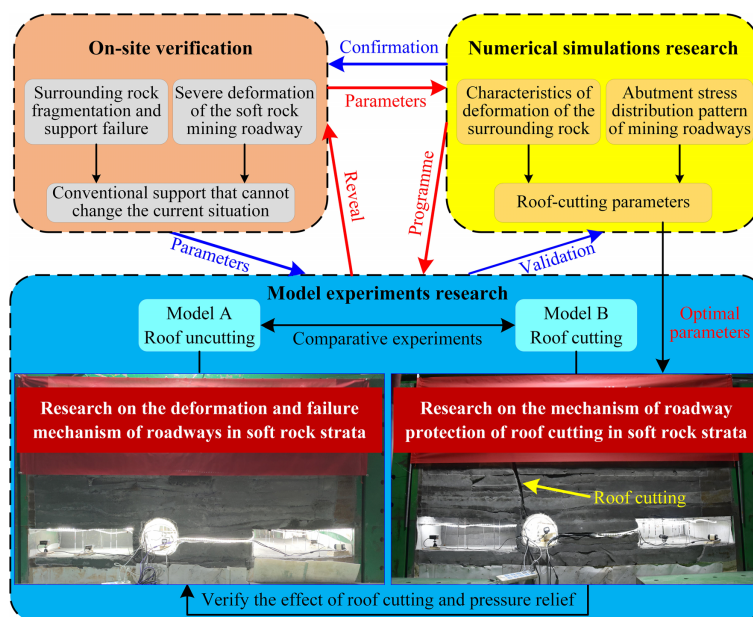


FIGURE 4 Research methods and relevance.

equation, geometric equation and physical equation (Xue et al., 2022; Zhu et al., 2022c). The boundary conditions should also be similar, and the similar scale of dimensionless physical quantities should be equal to 1 (Jongpradist et al., 2015). The similarity relationships of various physical parameters are calculated through similarity criteria (Table 3).

The simulation range of the model experiment is calculated based on the size and geometrical similarity scale of the model experimental device. The engineering prototype mainly includes four types of rocks (coal, mudstone, sandy mudstone, and fine sandstone). Although each type of rock is in different strata, its lithology is similar. Most rocks have low uniaxial compressive strength and are typically soft rocks, increasing the difficulty of selecting similar materials. By investigating several cases and accounting for the construction method, material cost and safety of the physical model (Castro et al., 2007), the mixed material was finally chosen. The mixed material consists of iron powder, barite powder, quartz sand, gypsum powder and water. Adjusting the ratio of various materials can change the physical parameters and improve the applicability of the materials (Zhu et al., 2022b).

Standard rock mechanics samples were made in groups according to different material proportions and dried naturally. Through indoor experiments, the mechanical properties of each set of samples were tested to find the optimal ratio to simulate different types of rocks (Figure 5). The mechanical properties of similar material tests should comply with the parameters calculated by similar scales. The parameters of four similar materials for typical rock stratum are shown in Table 3. The similarity ratio of geometry size C_L was set to 20. Mainly, the similarity of key parameters is ensured. Similar materials contain iron powders, so their unit weight is greater than that of the original rock. The similarity ratio of density C_γ was 0.79. The model similarity relationship and parameters of similar materials of typical rocks are illustrated in Table 1. Mechanical tests were carried out on similar support materials (Zhu et al., 2022a), and support components similar to the “bolt-cable mesh-shotcrete + steel belt” were obtained (Figure 5).

3.3 Model sensor placement

The size of the experiment was 2280 mm × 1000 mm × 2280 mm, length × width × height (Figure 6A). There are three

monitoring sections in the similar surrounding rock (sections I-III) and the internal model roadway (section IV-VI). The spaces between the sensor and the similar roadway surface are 0.1H, 0.5H and 1.0H, and H is the height of the roadway (Figure 6B). The microconvergence meter is set to monitor the internal similar roadway convergence (Figure 6C).

3.4 Embedded device for the model experiment

The model roadway is made of similar support materials, and the shape is controlled by a special mold (Shimamoto and Yashiro, 2021). A layer of clingfilm was wrapped around the outer side of the special mold for the easy removal of inner fillers at a later stage. A layer of gypsum was evenly applied to the outer side of the clingfilm to simulate secondary shotcrete. After drying the gypsum, the metal mesh, model bolt, and cables were set up. Finally, a second layer of gypsum was applied to the outer side of the metal mesh to simulate the initial shotcrete. The structure is equivalent according to a similar scale (Zhu et al., 2023). The interior of the model roadway is a removable filling structure, and the exterior is a similar composite structure of “bolt-cable mesh-shotcrete + steel belt” (Figure 7A).

The model gob is a three-layer structure of “lower board + support board + upper board” (Figure 7B). The support boards were divided into two types, with a thickness of 20 mm. The main support board was temporarily fixed with a small quantity of glue, the auxiliary support board was located between the two main support boards, and the upper part of the auxiliary support board was provided with circular holes for the iron wires. The preembedded device of similar roof cutting was a combined structure composed of two layers of aluminum plates (thickness of 0.5 mm) sandwiching steel wire (diameter of 2.2 mm), as illustrated in Figure 7C. The length of the roof cutting device is 400 mm, which is consistent with the length of goaf A. The height of the roof cutting device is 500 mm, which represents the actual cutting height of 10 m. After the removal of the steel wire, there was a gap between the two aluminum plates, which is equivalent to roof cutting. The spatial positions of the three embedded devices in the physical model are consistent with the engineering background (Figure 7D). After the removal of goaf A in the physical model, the

TABLE 3 Similarity ratio and similarity materials of the model experiment.

Similarity parameters	Symbol	Relations	Value	Similarity materials			
				Sandy mudstone	Fine sandstone	Mudstone	Coal
Density	C_γ	$C_\gamma = \gamma_b / \gamma_M$	0.79	2531 kg·m ⁻³	3015 kg·m ⁻³	2571 kg·m ⁻³	1718 kg·m ⁻³
UCS	C_σ	$C_\sigma = C_L C_\gamma$	15.8	0.521 MPa	1.256 MPa	0.744 MPa	0.819 MPa
Cohesion	C_c	$C_c = C_\sigma$	15.8	0.161 MPa	0.256 MPa	0.23 MPa	0.057 MPa
Poisson's ratio	C_μ	$C_\mu = C_c$	1	0.25	0.19	0.21	0.28
TS	C_σ	$C_\sigma = C_L C_\gamma$	15.8	0.063 MPa	0.136 MPa	0.061 MPa	0.055 MPa
EM	C_E	$C_E = C_L C_\gamma$	15.8	0.119 GPa	0.605 GPa	0.182 GPa	0.213 GPa
Friction angle	C_θ	$C_\theta = C_\mu$	1	18°	31°	20°	29°

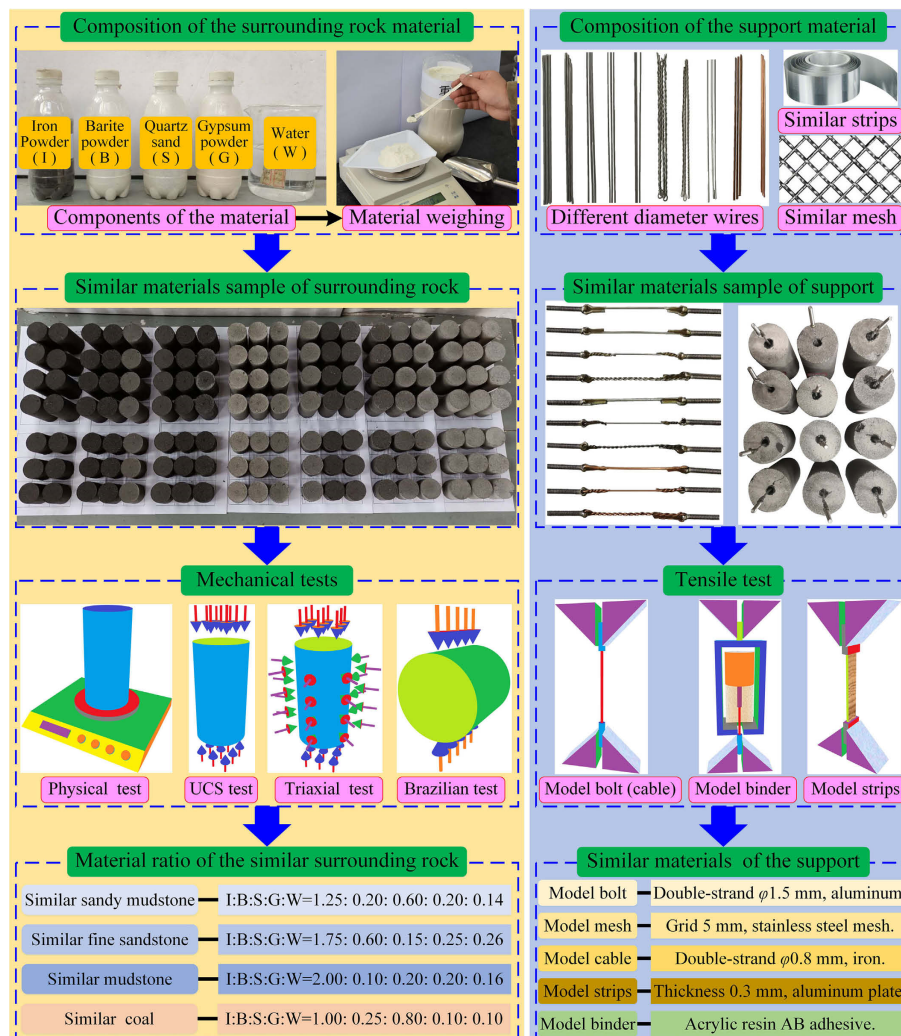


FIGURE 5 The selection process of the model experiment materials.

longwall face is 400 mm away from the front boundary. This ensures that the progress of panel mining and roof cutting is consistent. Due to the limitations of the experimental conditions, in this model, the experiment is performed equivalently. The physical model simulates the coal mining process through prefabrication and demolition and uses a step-by-step loading stress to model the increase in abutment stress under coal mining conditions.

3.5 The process for the model experiment

It is difficult to construct model panels, gobs and roadways by conventional methods. For this reason, we innovated the model construction process initially by prefabrication and then by dismantling. To reduce the friction effect of the boundary, polytetrafluoroethylene (PTFE) plates were set on the surface of the model. After the model stress was stabilized, the next load was applied (Arora et al., 2022). The coal dip is equivalent to a

horizontal structure, and the physical model was made layer by layer. The construction process was divided into eight steps. To show the inner construction process of the physical model, the front panel of the test device is not illustrated in steps 2-4.

Step 1: The upper steel beam of the experimental device was removed, and the physical model was constructed layer by layer from the bottom up. The drying time of each layer was 24 h.

Step 2: The grooves were excavated, and the sensors were installed according to the monitoring plan.

Step 3: The coal pillar and panels in the model were made, and gob A, gob B and the model roadway were preembedded. After the model was constructed for the location where the roadway was to be installed, grooves were made according to the shape of the roadway floor. During the installation of similar bolts, the drill holes were cleaned, and adhesive was injected into the holes. The remaining model cables and bolts were buried in similar materials in the surrounding rock using artificial construction methods. Roof cutting device at the upper left position of the model roadway along the coal mining direction, with a length of 40 cm (Figure 8A).

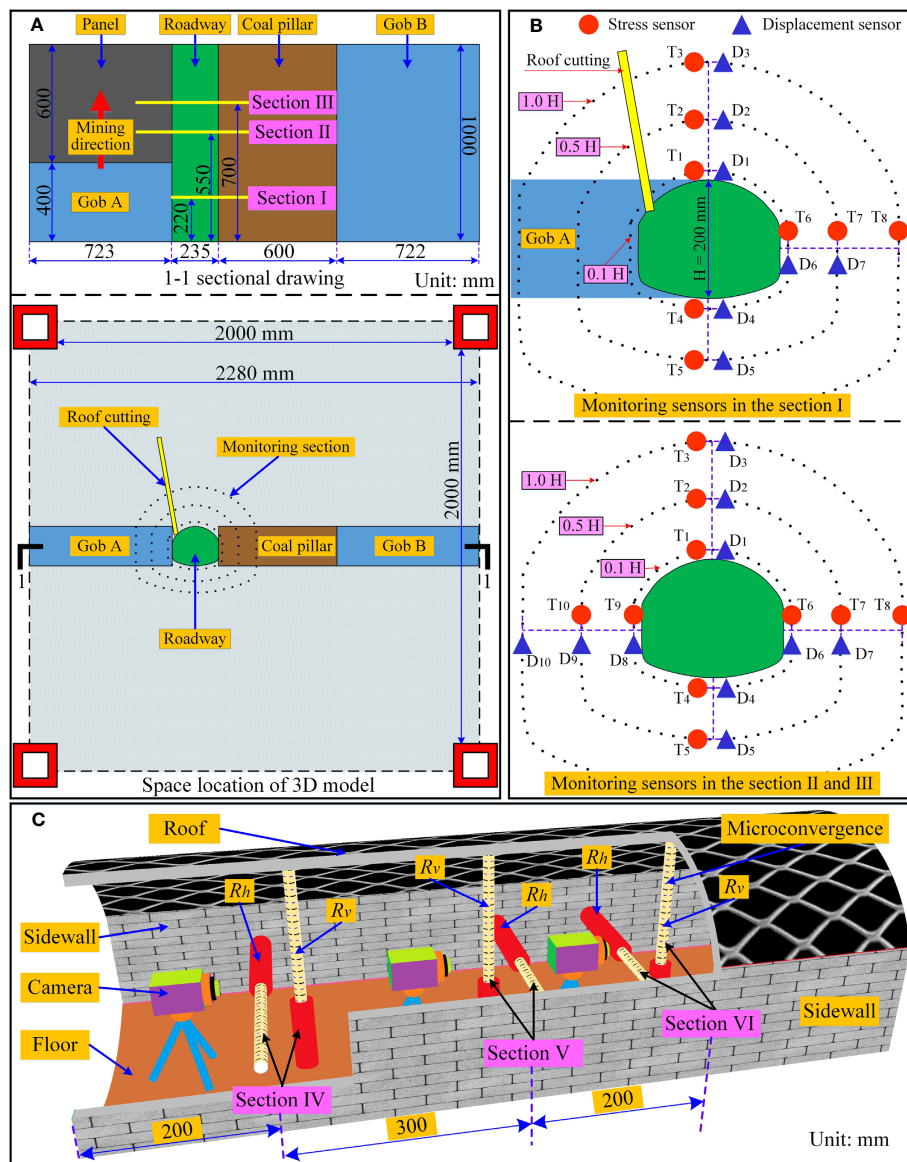


FIGURE 6 Monitoring sensor locations. (A) Monitoring section position. (B) Monitoring sensors in sections I-III. (C) Monitoring sensors in sections IV-VI.

Step 4: A similar roof cutting device was aligned with the model roadway prefabricated crack, which was preembedded into the surrounding rock during the layer-by-layer construction process. The model was continually manufactured to the design height.

Step 5: After the model was completely dry, the top force transmitter and reaction beam were installed, and the front panel was removed (Figure 8B).

Step 6: The support boards and the upper and lower boards of similar gob A and gob B were removed. The fillers of the model belt roadway were removed, and the interior space of the roadway was restored. The wire was pulled out to form a similar roof cut.

Step 7: Microconvergence meter instruments and cameras were installed in the model roadway, and a flexible light-emitting-diode strip was used for lighting (Figure 8C).

Step 8: A PTFE plate was placed on the front of the physical model, and the front panel was reinstated. Various monitoring instruments and acquisition equipment were connected.

A 3D numerical model was constructed, and the stress within the model was set to the same value based on the measured *in situ* stress conditions. The numerical model simulates the mining process, and the range of simulations within the model ($45.6 \text{ m} \times 45.6 \text{ m} \times 20 \text{ m}$) was chosen based on C_L . Based on C_σ the stresses in different zones of the simulation range were calculated and reduced to the loading applied to the surface of the physical model ($2.28 \text{ m} \times 2.28 \text{ m} \times 1.00 \text{ m}$). The stress of the different paths on the physical model surface was controlled step by step according to the minimum accuracy of the servo loading system, and each load level was maintained for 4 h. After 18 steps (72 h), the model stress

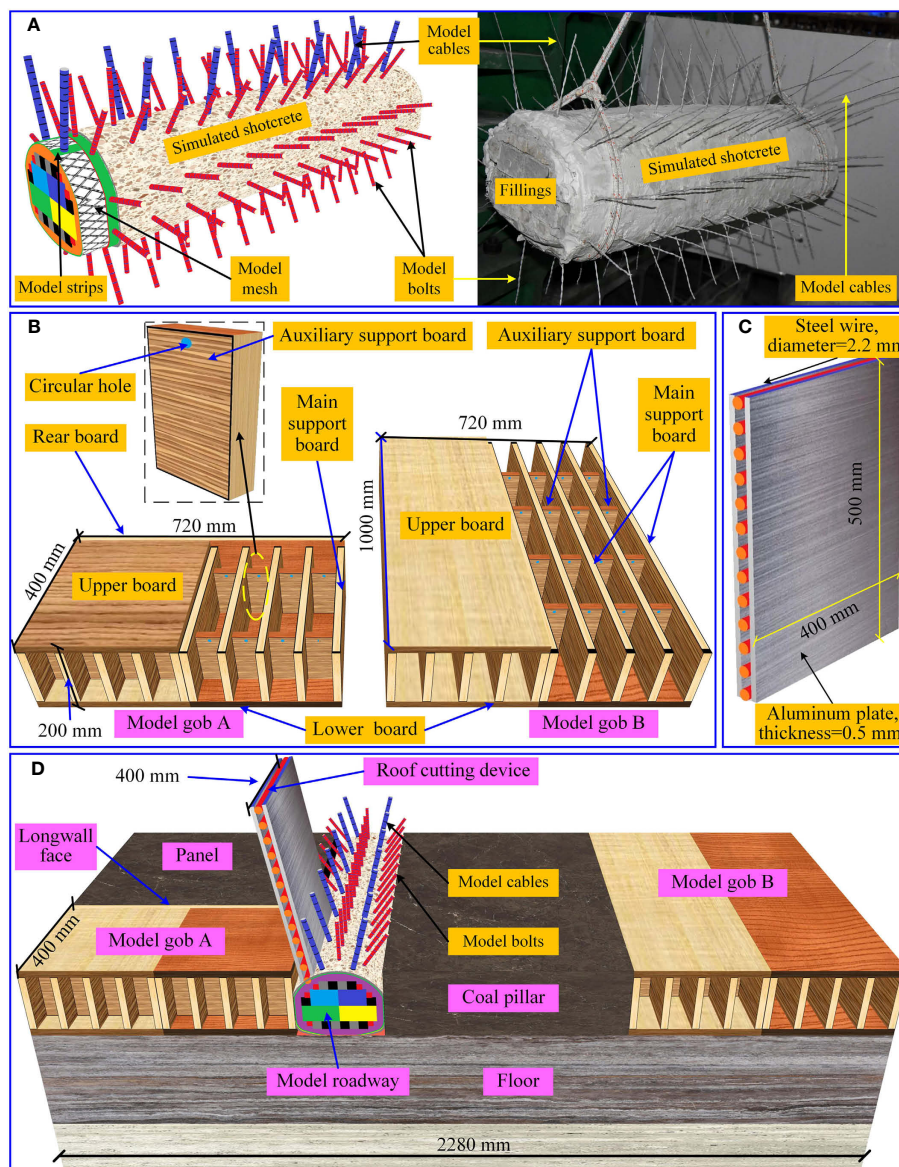


FIGURE 7 Similar device for the model experiment. (A) Similar "shotcrete + bolt-mesh-cable + steel strips" support. (B) Components of the similar gob. (C) Roof cutting device. (D) Relative position of embedded devices.

conditions were reached (Figure 9). The overload was then continued proportionally, and the failure characteristics of the roadway were simulated under increased mining stress (Tian et al., 2021; Zheng et al., 2021).

4 Results and analysis for the model experiment

The boundary stress was applied step by step according to the abovementioned ratio (Fang et al., 2023; Zhu et al., 2023). The experimental results are quantitatively described in terms of the top boundary stress of the physical model. The absolute values of deformation indicate the magnitude, which is positive toward the

center of the roadway. Negative values of the abutment stress of the surrounding rock indicate compression. Based on the deformation rate, this compression includes the initial stage, the rapid rising stage and the slow rising stage, corresponding to stages ①, ② and ③, respectively.

4.1 Deformation pattern of the surrounding rock

Section I is in the gob. In stage ①, the floor deformation is larger than that of the roof (Figure 10). The deformation of the right coal pillar is relatively small. In stage ②, the roof and the right sidewall are consistent and increase linearly. The line of demarcation of

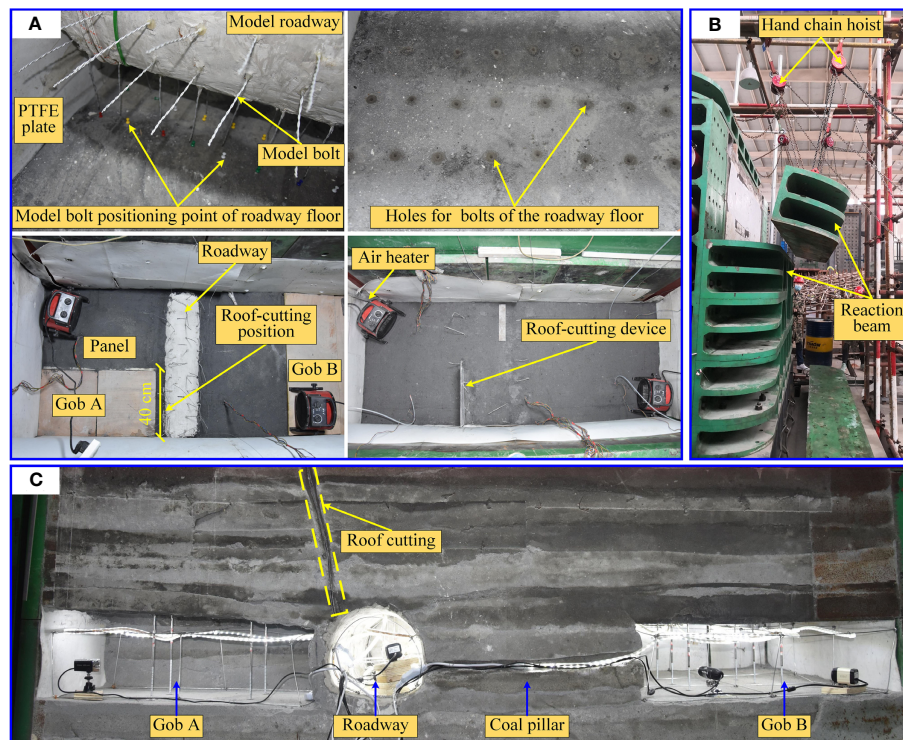


FIGURE 8
The procedure of the model experiment. (A) The preburial process of the model roadway and gob. (B) Installation of the reaction beam. (C) Installation of the microconvergence meter and cameras.

stages ③ and ④ is about 1.2 MPa. In stage ④, the increments of deformation of the roof, floor, and right sidewall are 48.4 mm, 21.02 mm, and 15.14 mm, respectively. The damage to the roadway in stage ④ is obvious, and the increments of the three parts account for 77.14%, 83.68% and 56.14% of the total. In stage ⑤, the average increment of deformation is only 4.85 mm. The deformation of the right sidewall is relatively large, and the vertical convergence is extremely small. The deformation patterns at different depths of the floor and sidewalls are similar. The deformation of the roof at the 0.5H and 1.0H positions is relatively small compared with that at the 0.1H position.

Section II is near the roof cut. The separatrix between the roof and floor deformation is 1.25 MPa and 1.50 MPa. In stage ①, the vertical convergence exceeds 12 mm, with the roof deforming more than the floor (Figure 11). The deformation of the roof at the 0.1H position increases linearly. In stage ②, the deformation of the roof increases by 25.87 mm, and the deformation of the floor increases by 14.51 mm. The deformation pattern at 0.5H position of roof is consistent with that at the 0.1H position. In stage ③, the deformation of the sidewall increases linearly. Above 1.25 MPa, the deformation increases rapidly. In stage ④, the increment of deformation of the left sidewall is 17.75 mm, which is 1.98 times larger than that of the right sidewall. In stage ⑤, the average increase in sidewall deformation is 3.76 mm. The deformation pattern at the 0.5H and 1.0H positions of the left sidewall is

consistent with the 0.1H position, and the left sidewall is the most severely damaged.

The pressure relief effect of the surrounding rock diminishes as it moves away from the roof cut. The roadway roof and floor consist of two stages, with boundary stresses of approximately 1.50 MPa and 1.69 MPa at the separatrix (Figure 12). In stage ①, both the roof and floor deformations demonstrate an increased concave shape. In stage ②, the vertical deformation increases linearly. The average growth rate of stage ② is 4.44 times that of stage ①. The sidewall deformation of section III can be divided into three stages, with stresses of 1.25 MPa and 1.75 MPa at the separatrix. The deformation of the left sidewall is 1.48 multiples that of the right, and the average deformation rates of stages ③ and ④ are 5.01 multiples and 1.62 multiples that of stage ①, respectively.

4.2 Evolutionary pattern of abutment stress

The abutment stress in each section of the roadway does not always increase. To describe the characteristics of abutment stress, according to the rate of change at the 0.5H position, the stress process can be divided into the growth stage (stage ①), the release stage (stage ②) and the adjustment stage (stage ③). The abutment stress in stage ③ reaches its peak value, and the average boundary stress is 1.15 MPa.

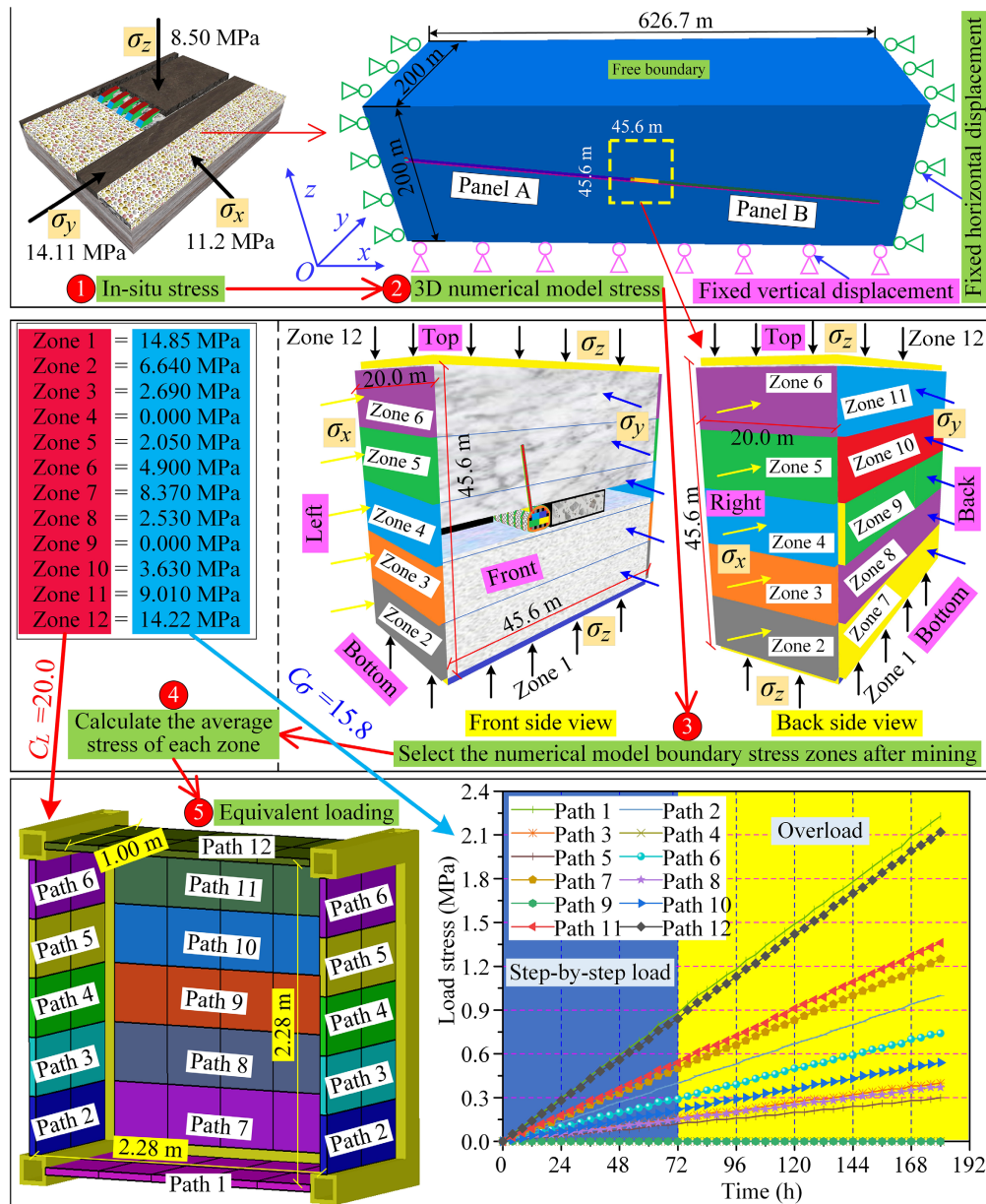


FIGURE 9 Physical model boundary stress application process.

In section I, the roof abutment stress is relatively small. The maximum abutment stress at the 0.1H position of the roof is only 0.2 MPa. With the increase in deformation, the roof stress is continuously loosened until it drops to zero. The maximum roof abutment stress in the 0.5H position is 0.6 MPa, which is reduced by 0.2 MPa in stage ©. The roof abutment stress at the 1.0H position has no significant release stage, with a maximum value of approximately 0.95 MPa (Figure 13). The pattern of the right sidewall is the same as that of the roadway roof. The abutment stress at the 0.1H position can also be divided into three stages. The roof cutting reduces the load of the coal pillars, but the right coal pillar still bears the stress of the roadway roof and the overlying

strata. The coal pillar abutment stress is small in the shallower part of the right sidewall and relatively large at the 1.0H position. The floor support strength is higher than that of the roadway roof, so the abutment stress of the floor at the same depth is greater than that of the roof. With a further increase in the floor deformation, the floor stress is released. The amplitude of the drop at 0.5H position of floor is approximately 0.2 MPa.

The roof deformation at the rear of the longwall face pulls the roof stratum in front to move downward, resulting in a continuous increase in the abutment stress of the section II roof. In stage ©, the maximum abutment stress at the 0.1H position of the roof is 0.32 MPa (Figure 14). In stage ©, the maximum reduction in stress at the 0.1H position of the

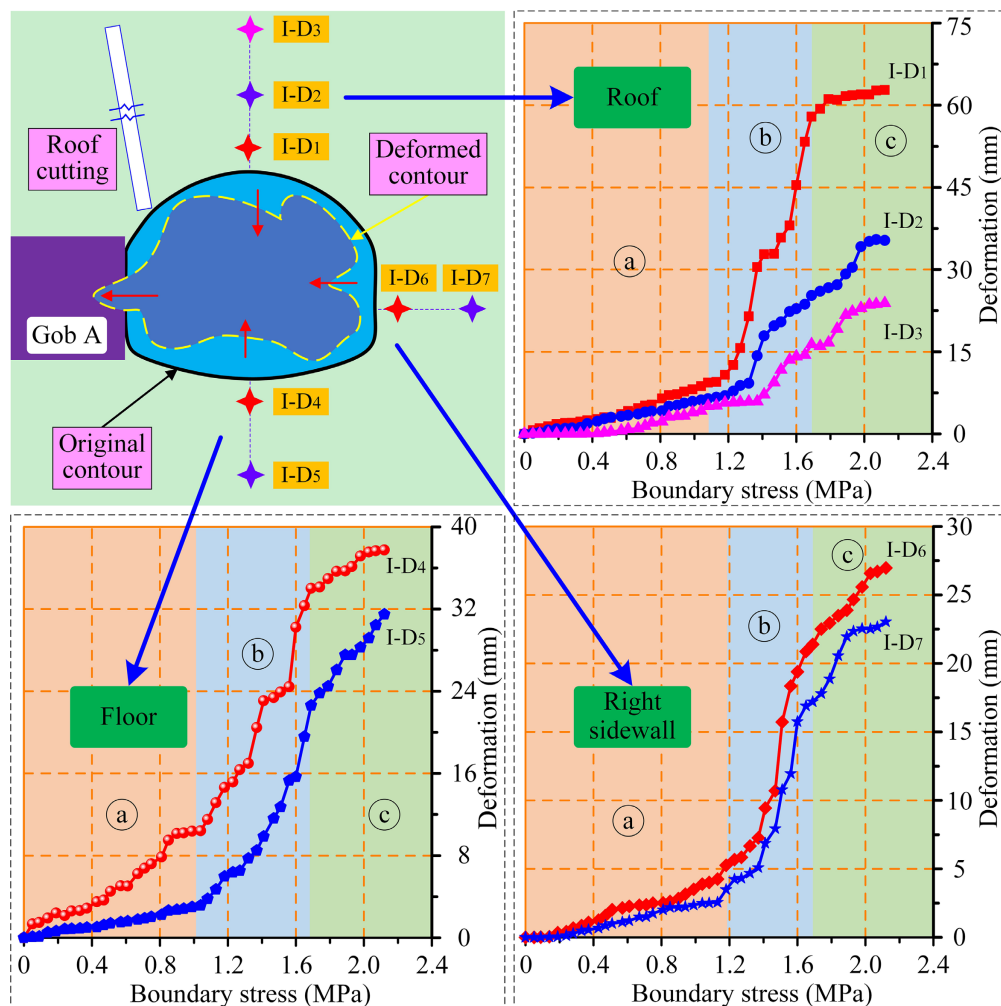


FIGURE 10 Deformation of section I.

roof is 84.4%. The roof abutment stress at the 1.0H position increases continuously and reaches a peak value of 2.4 MPa. The abutment stress at the 0.1H position of the sidewall shows a three-stage pattern of change, but stage © of the left sidewall is relatively short. As the deformation continues to increase, the abutment stress of the left sidewall does not decrease significantly but continuously adjusts. In stage ©, the abutment stress at 1.0H position of the right sidewall increases continuously and reaches a peak value of 2.47 MPa. The pattern of the floor abutment stress at the 0.1H position is similar to that of section I. In stage ©, the floor stress is obviously diminished, with a maximum decrease of 0.49 MPa. In stage ©, the abutment stress of the floor increases slowly.

The roof abutment stress at 0.5H position has no significant release stage, and it still increases gradually in stage © (Figure 15). The maximum roof abutment stress at the 1.0H position reaches 3.42 MPa, which is 1.6 multiples the upper boundary stress. The abutment stress at the same position of floor is similar to that of roadway roof. In stage ©, there is no obvious stress release stage for

the abutment stress at the 0.1H and 0.5H positions of two sidewalls. In stage ©, the average abutment stress of the sidewalls is 1.04 MPa, and there is no obvious difference between the two sidewalls. As the loading stress increases, the roadway at the 0.1H position of the sidewall is destroyed, and its abutment stress drops to 0. The abutment stress in the 1.0H position of the right sidewall increases linearly with the boundary stress.

4.3 The convergence features of the mining roadway

The mining roadway converges inward and squeezes the composite support structure. Damage to the interior of the roadway primarily consists of shotcrete cracking, spalling and metal mesh bending (Figure 16A). With 0.51 MPa as the dividing line, roadway convergence is divided into a slow stage and a rapid stage according to the vertical rate of change (Figure 16B). The

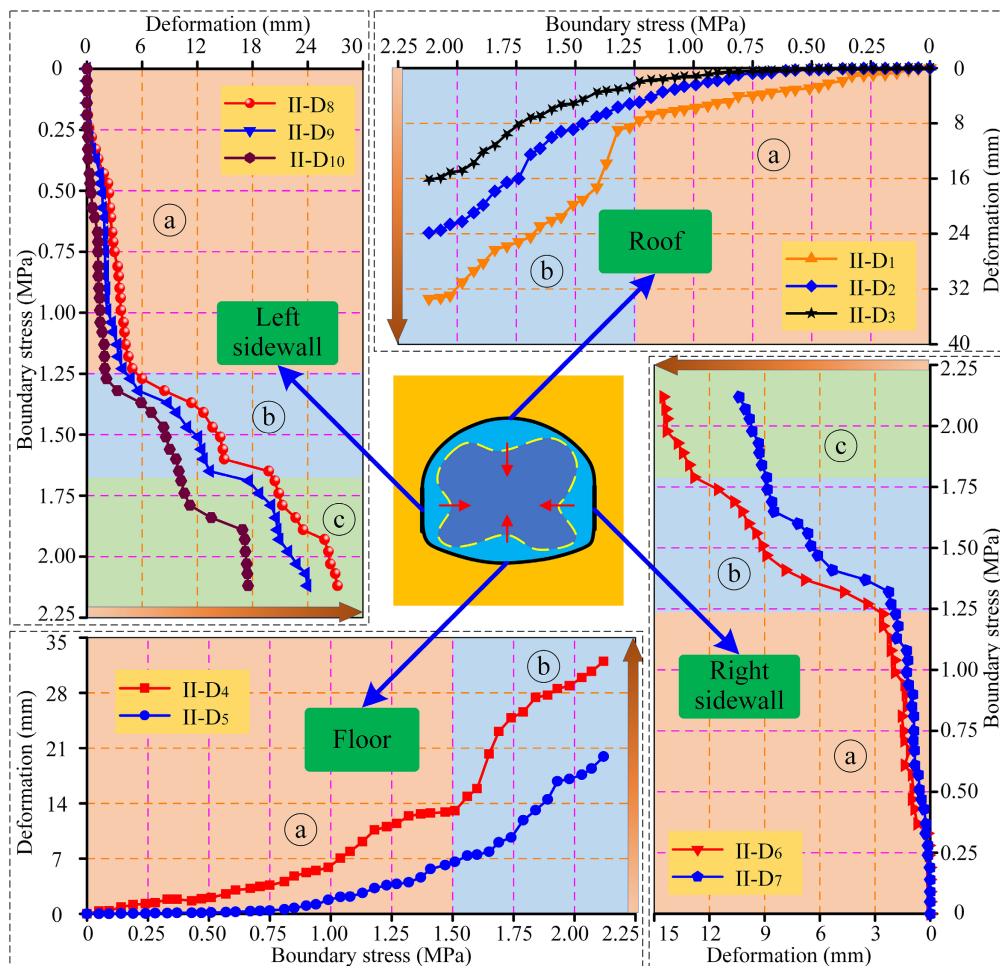


FIGURE 11 Deformation of section II.

average convergence rate of change in the slow stage is 11.16 mm/MPa and that in the rapid stage is 34.93 mm/MPa. The left of section IV is the model gob, where the roof of the roadway is presplit and the vertical convergence deformation is the largest. Section V is in front of section IV and near the longwall face. Section VI is the farthest from the mining face, and the vertical convergence is relatively small. At a boundary stress of 1.69 MPa, the convergence values are 59.33 mm, 46.23 mm, and 36.22 mm for sections IV-VI, respectively.

5 Numerical simulation research

5.1 Numerical model construction

A 3D numerical model was constructed using FLAC3D based on the belt roadway at the Xinshanghai No. 1 Coal Mine. The numerical model includes coal pillars and two gobs, and the inclination angle of the coal formation is 6° (Figure 17A). To

improve the calculation accuracy, the grid near the roadway is densified (Li et al., 2022b). The constitutive model is the Mohr-Coulomb model (Li et al., 2022c; Najm and Daraei, 2023). The boundaries around the model and the bottom are constrained, and the top is free. Coal mining and roof cutting use null elements (Zhang et al., 2023). In this section, the same three sections as those in the model test and section D behind the longwall face are chosen for analysis (Figure 17B).

5.2 Vertical deformation of the surrounding rock

The vertical convergence of the roadway increases continuously from section III to section D (Figure 18). The vertical deformation of section III is approximately 147 mm, which is 29.32% less than that of section II. When the roadway is located at the gob, there is no coal seam support on the left side of the roadway, and the vertical deformation of the gob converges suddenly. The vertical

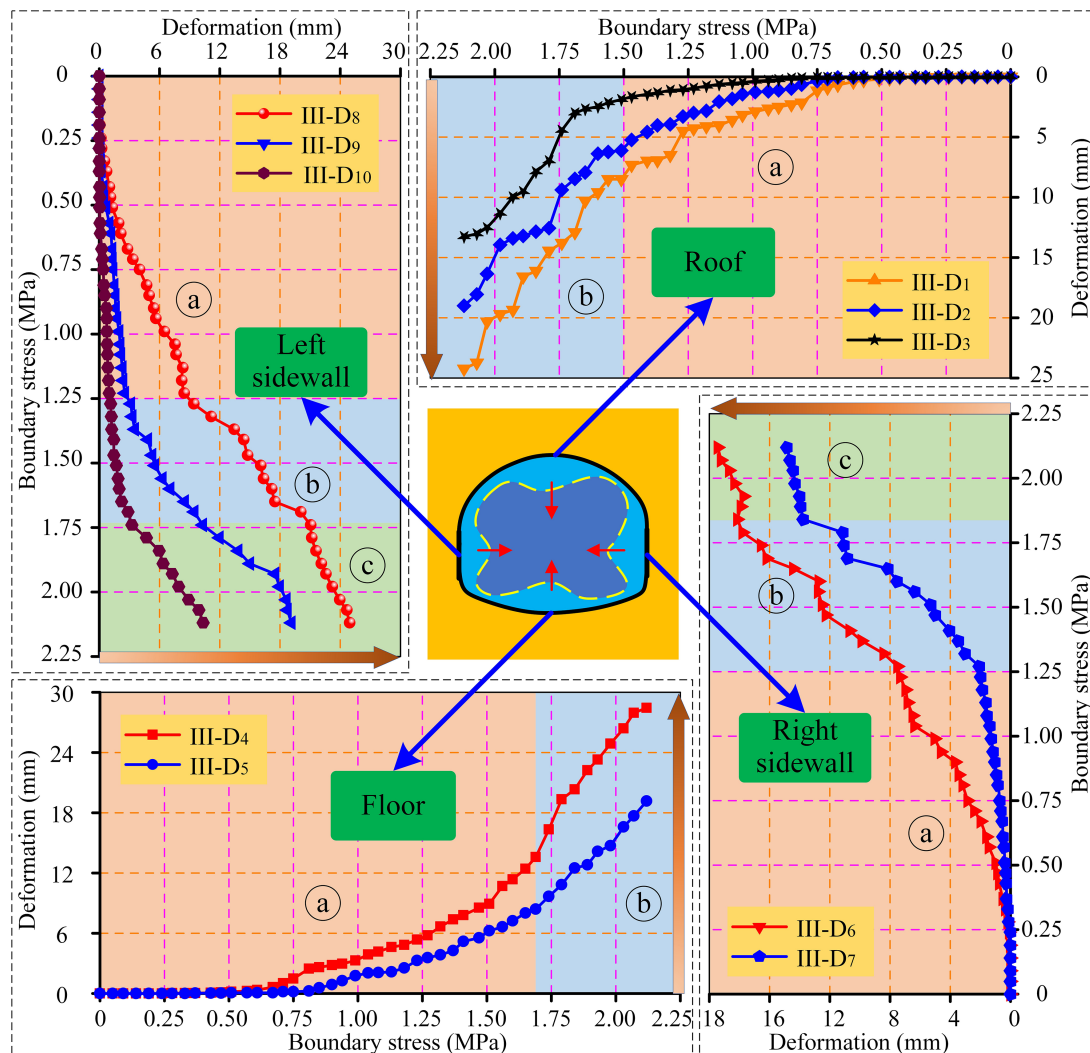


FIGURE 12 Deformation of section III.

deformation of section I is approximately 341 mm. Approximate amounts of roof and floor deformation in section III are reduced by 27.4% compared to the roadway without roof cutting. The floor of the gob and roadway in section D is severely heaved, and the vertical deformation of the roadway is more than 500 mm.

5.3 Abutment stress of the surrounding rock

There is a significant stress concentration area in the left sidewall of section III, with a peak stress of 22.5 MPa, and the minimum spacing between the stress concentration zone and the roadway is about 4 m (Figure 19). The abutment stress of the right coal pillar is smaller than that of the left sidewall, i.e., approximately 20.0 MPa, and the roof abutment stress is much greater than that of the roadway floor. The roadway roof stress of

section III is reduced by 9.77% compared to that of the roadway without roof cutting, and the stress on the right coal pillar is reduced by 15.38%.

A maximum value of the left coal seam of section II is 27.5 MPa. Compared to the roadway without roof cutting, the stress on the left side of section II is increased by 10%, and the stress on the right coal pillar is decreased by 11.1%. Coal mining leads to a sudden drop in the stress of the roof and floor of the gob and then affects the distribution of the roof stress of sections I and D. The roof abutment stress of the roadway in section I is transferred to the right coal pillar, forming a stress concentration area within 4.5 m of the right sidewall, with a peak stress of 26.9 MPa. The roof and floor strata of the gob in section D have a large-scale tensile zone. The roof cutting of the rear roadway results in stress transfer to the front panel roof, and the abutment stress within 0.5H of the roadway is less than 20.0 MPa. The reduction in stress is beneficial for the stability of mining roadways.

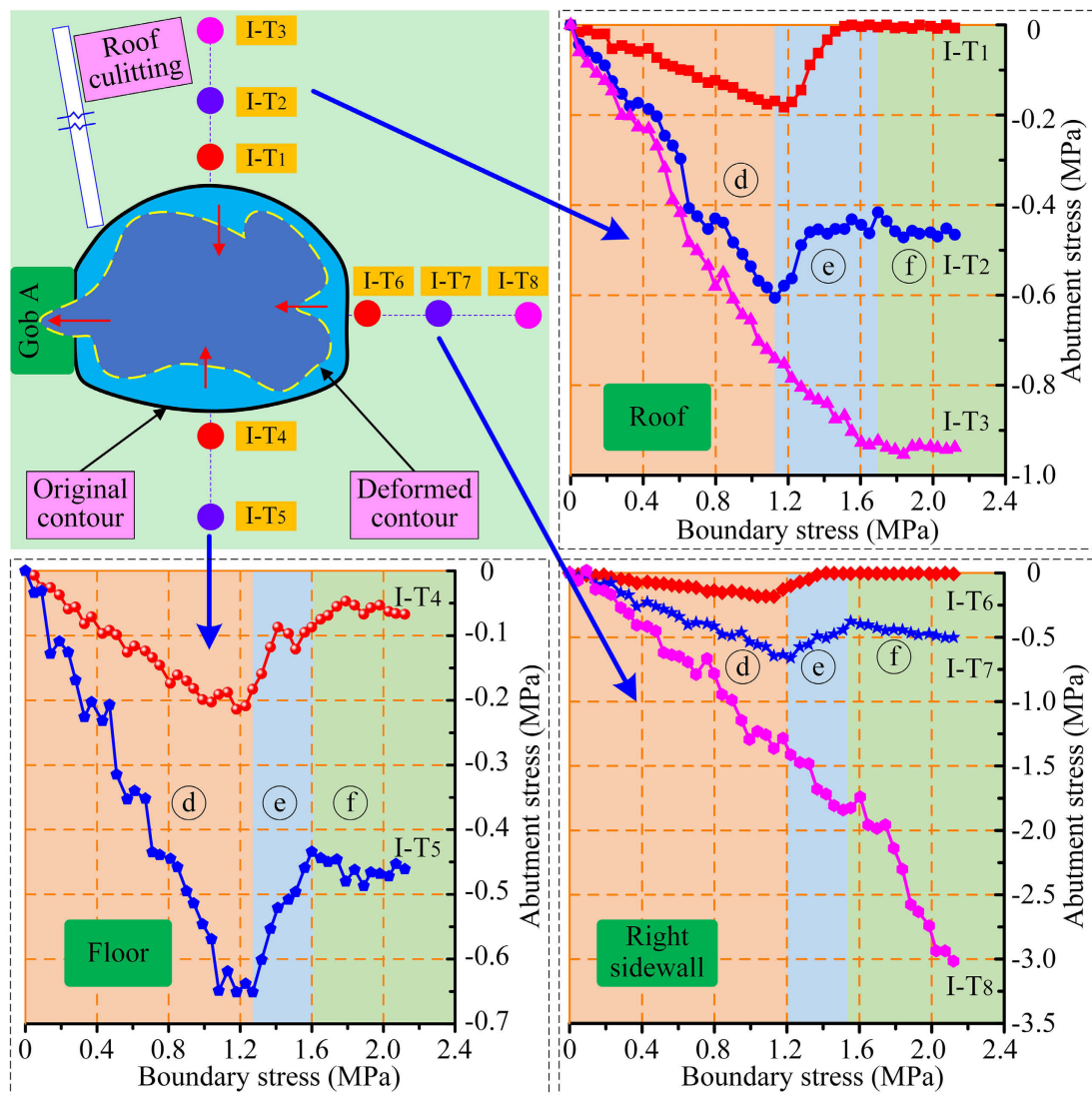


FIGURE 13
Abutment stress of section I.

5.4 Plastic zone

The plastic area increases continuously from section III to section I (Figure 20). The plastic area in the left sidewall of section III extends approximately 4.7 m, which is larger than that of the right sidewall. The plastic area of the floor is approximately 3.6 m larger than that of the roof. The plastic areas of the roof and the right sidewall of section II vary less, and the depth of damage to the floor increases. The left side of section II is severely squeezed and damaged by the action of high abutment stress. The maximum depth of the plastic area on the roof of section I is approximately 10 m upward, and the average depth on the floor and the right sidewall is 5 m. The plastic zone at the roof and floor level of the gob is significantly expanded to more than 10.5 m. Significant tensile–shear composite failure occurs in the roadway near the roof cutting.

6 Discussion

6.1 Comparison of the two model experiments

After the model experiment is complete, the physical model’s surrounding rock and roadway are excavated. Section I is in the gob and is the most deformed part of the two experiments (Figure 21). Roof cutting in the roadway caused the roof of the gob to collapse more fully. In monitoring section I of the roadway, the deformation of model B was greater than that of model A, suggesting that roof cutting accelerated the deformation of the surrounding rock behind the longwall mining face. However, the deformation of section III of the Model B (about 50 mm) roadway was smaller than that of Model A (about 61 mm), and the vertical

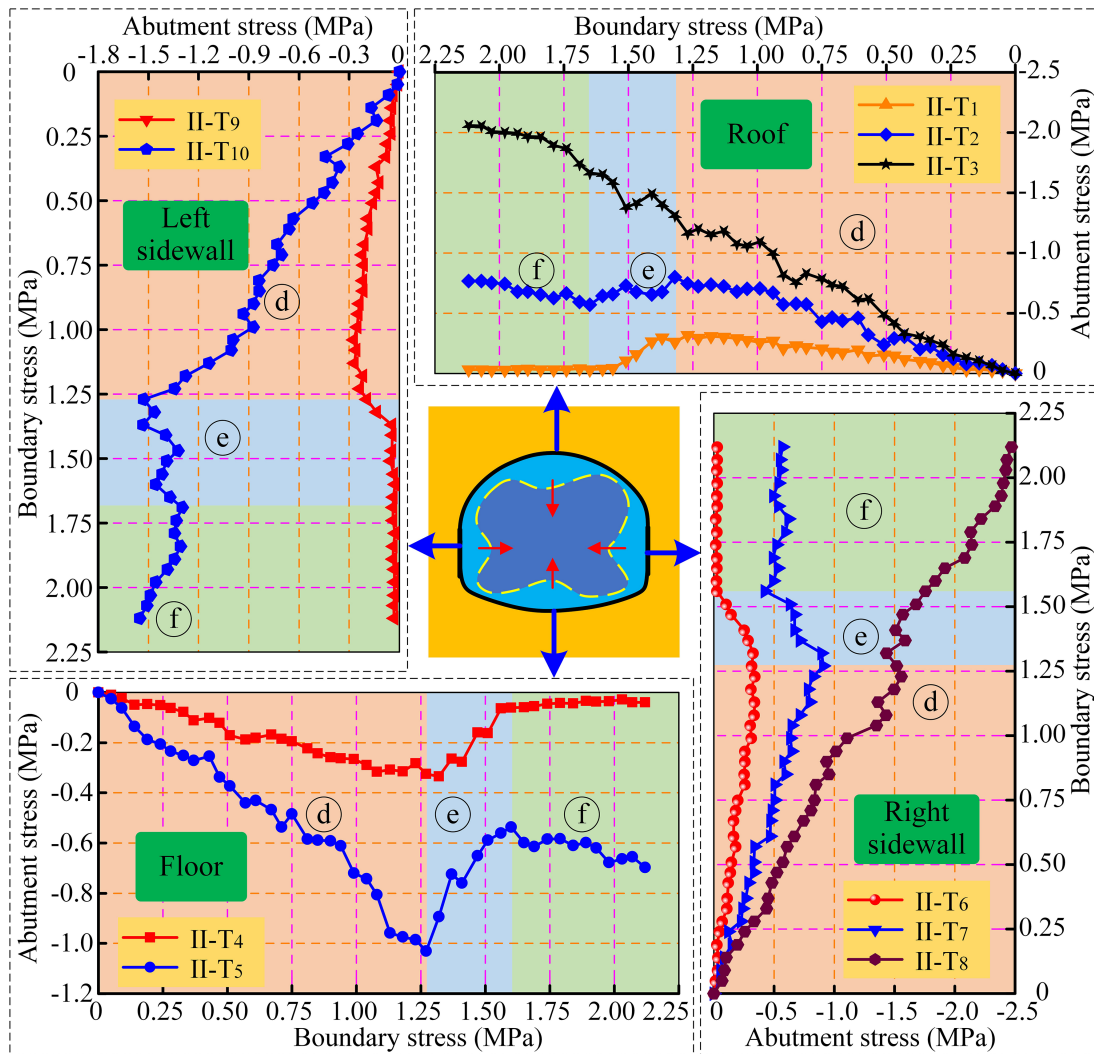


FIGURE 14
Abutment stress of section II.

size of Model B roadway increased by 7.91%. This can intuitively reflect the beneficial effect of roadway roof cutting. Through comparative experiments, it has been demonstrated that roof cutting without increasing the support structure can significantly reduce the deformation of the roadway in front of the longwall face and maintain the stability of the surrounding rock.

6.2 Mechanism of soft-rock roadway protection by roof cutting

Four sections (1-1, 2-2, 3-3, and 4-4) are selected to analyze the mechanism of soft-rock roadway protection by roof cutting

(Figure 22A). The mechanism and stress transfer process of roadway protection in soft-rock roadways are described as follows.

(1) Cut off the transverse connection to the stratum behind the longwall face and transfer the stress to the front coal seam.

The transverse connection between the roof of the gob and the roadway behind the longwall face within the range of the cut is removed, and the movements of the surrounding rock of the two roofs are independent of each other (Figure 22B). The pressure from the overlying strata in the gob is transferred to the fully mechanized mining support and the front coal seam. The cut decreases the extension size of the rear roadway roof, reduces the additional force on the roadway roof caused by the rotary subsidence of the gob roof, and reduces the abutment stress of the coal pillar (Yang et al., 2021). The stress transfer results in an increase of 10% in the roof stress of the coal in front of the gob

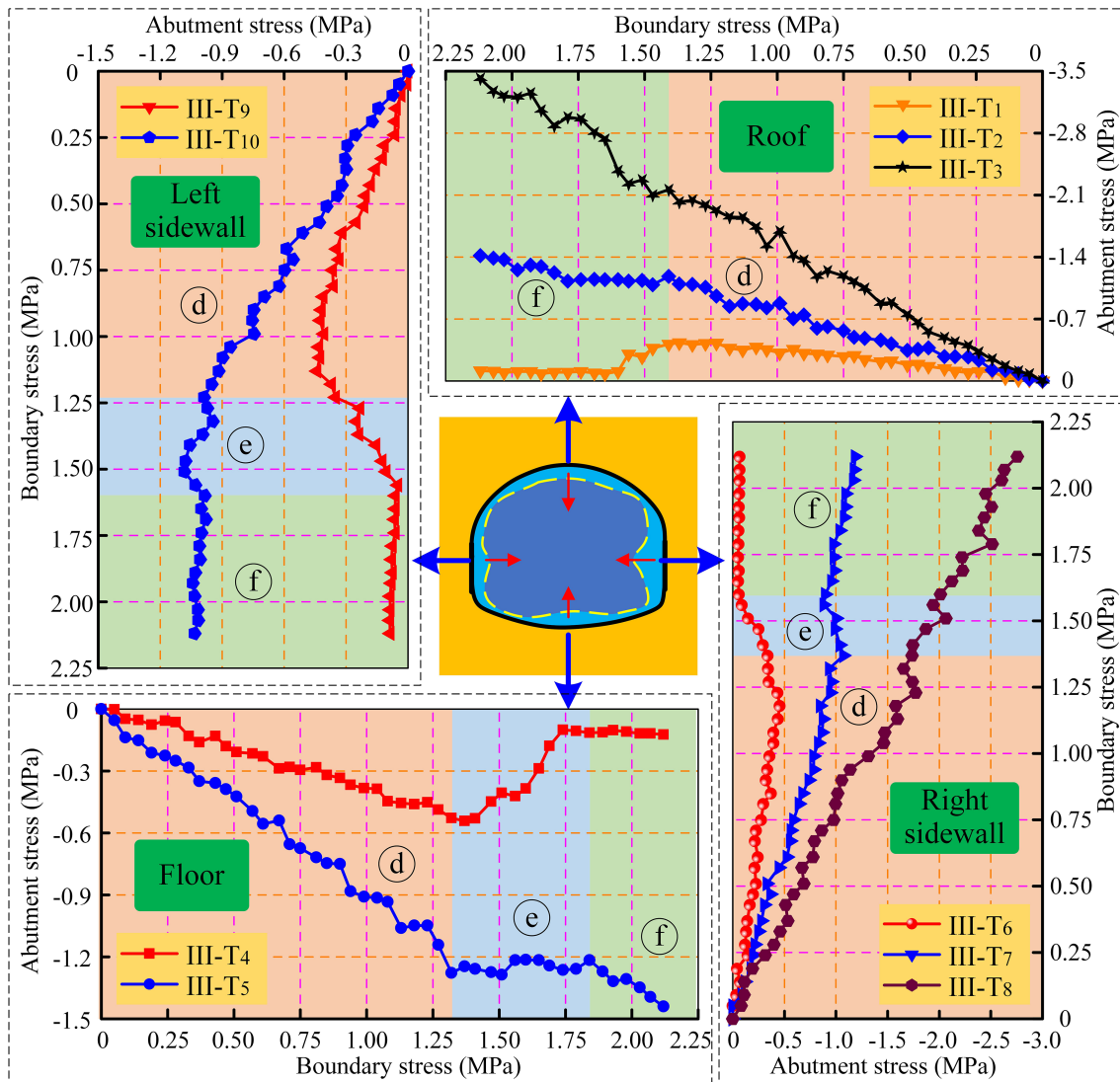


FIGURE 15 Abutment stress of section III.

(Figure 22C). The average stress in the roof of the rear roadway is reduced by 33%, and the average stress in the front roadway is reduced by 12.57%, except for the left sidewall.

(2) Weaken the longitudinal connection of the roof and reduce the deformation of the front roadway.

The gob roof deforms and collapses because of coal mining (Figure 22D). The collapse of the roof in the gob also causes part of the gangue to invade the abandoned roadway. As the gangue continues to compress and compact, it also plays a supporting role in the overlying strata. Different from the gob, hydraulic supports and original support structures are present in the roadway. The rock of the roadway is still mechanically connected in the longitudinal direction (mining direction). Since the movement of the surrounding rocks in the gob no

longer affects the roof of the rear roadway, the roadway is also deformed by the overlying strata (Figure 22E). In the mining direction, the deformation of the rear roadway is much larger than that of the front roadway. Due to the longitudinal connection between the rock formation and the supporting structure, the rear roadway also drags the front roadway as it deforms. The cut reduces the overall deformation of the rear roadway, weakens the traction effect, and reduces the front roadway deformation. The vertical convergence of the front roadway is reduced by 27.3%, and the coal pillar deformation is diminished by 15.7%.

(3) The stress distribution of the roadway is changed, and the average stress of the front roadway is reduced within the failure threshold.

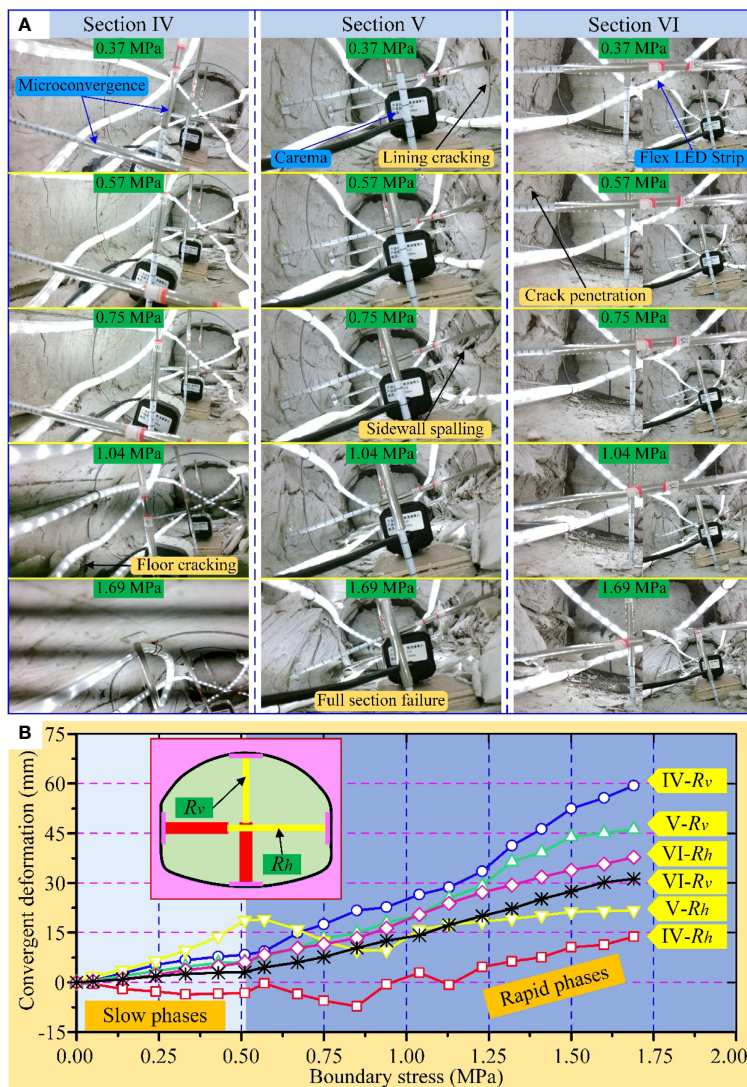


FIGURE 16 Deformation characteristics of roadway. (A) Failure mode. (B) Roadway convergence.

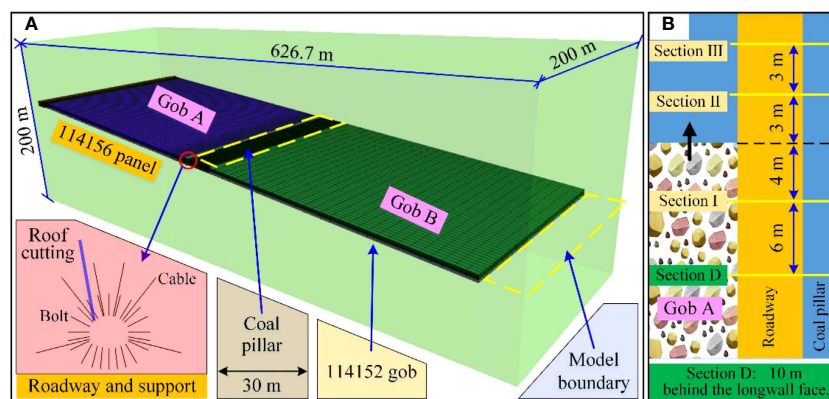


FIGURE 17 Numerical simulation model. (A) Numerical simulation model. (B) Section location.

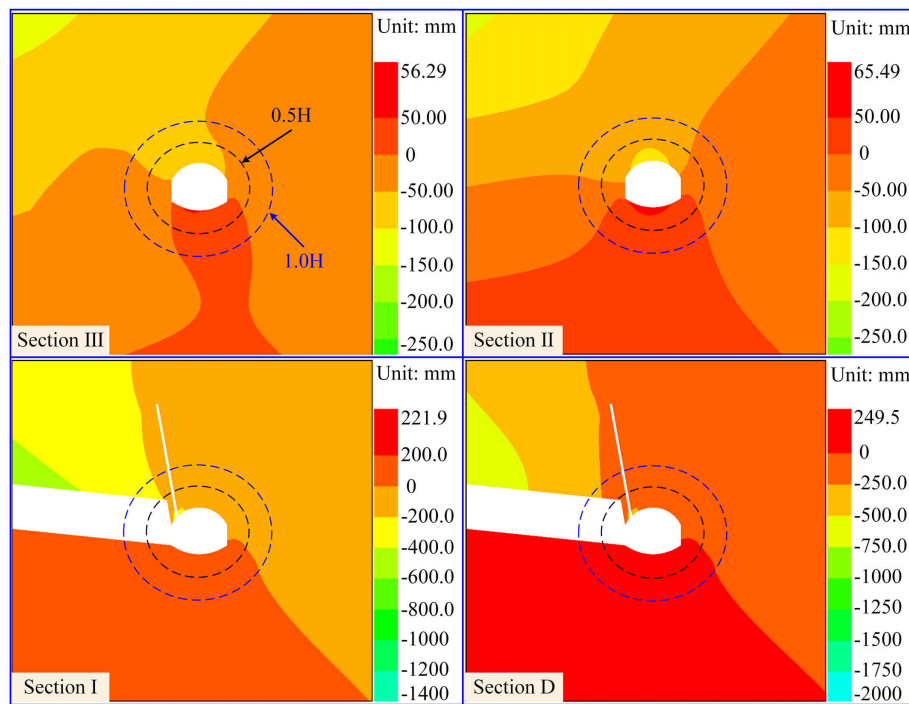


FIGURE 18 Characteristics of the roadway vertical deformation.

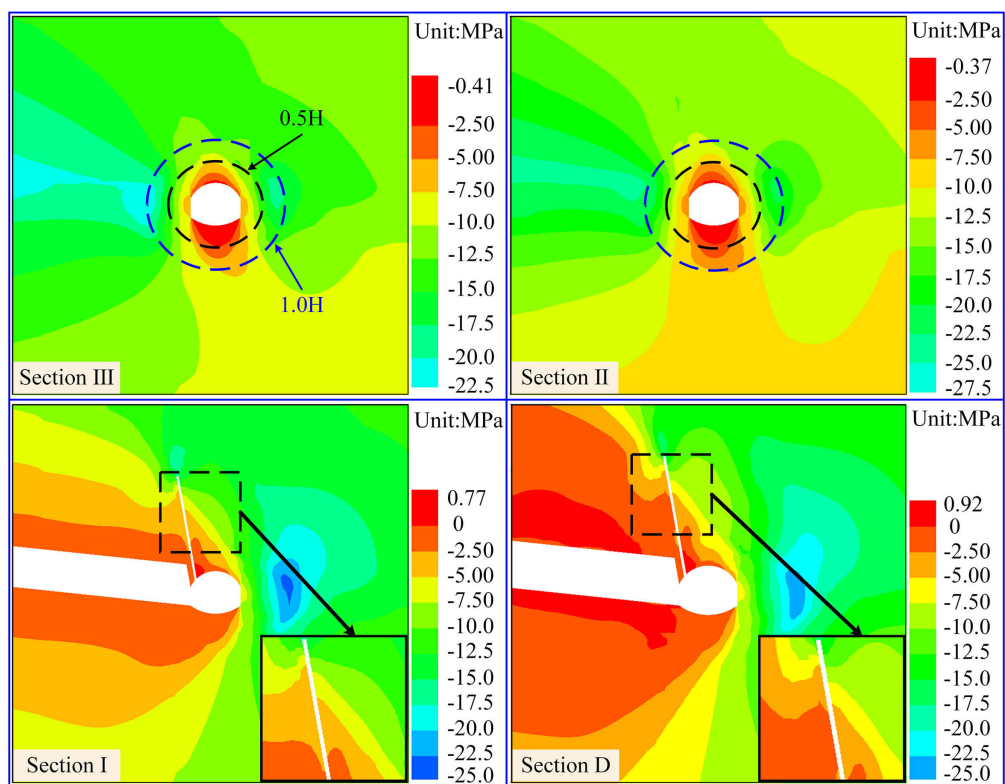


FIGURE 19 Distribution pattern of abutment stress in the roadway.

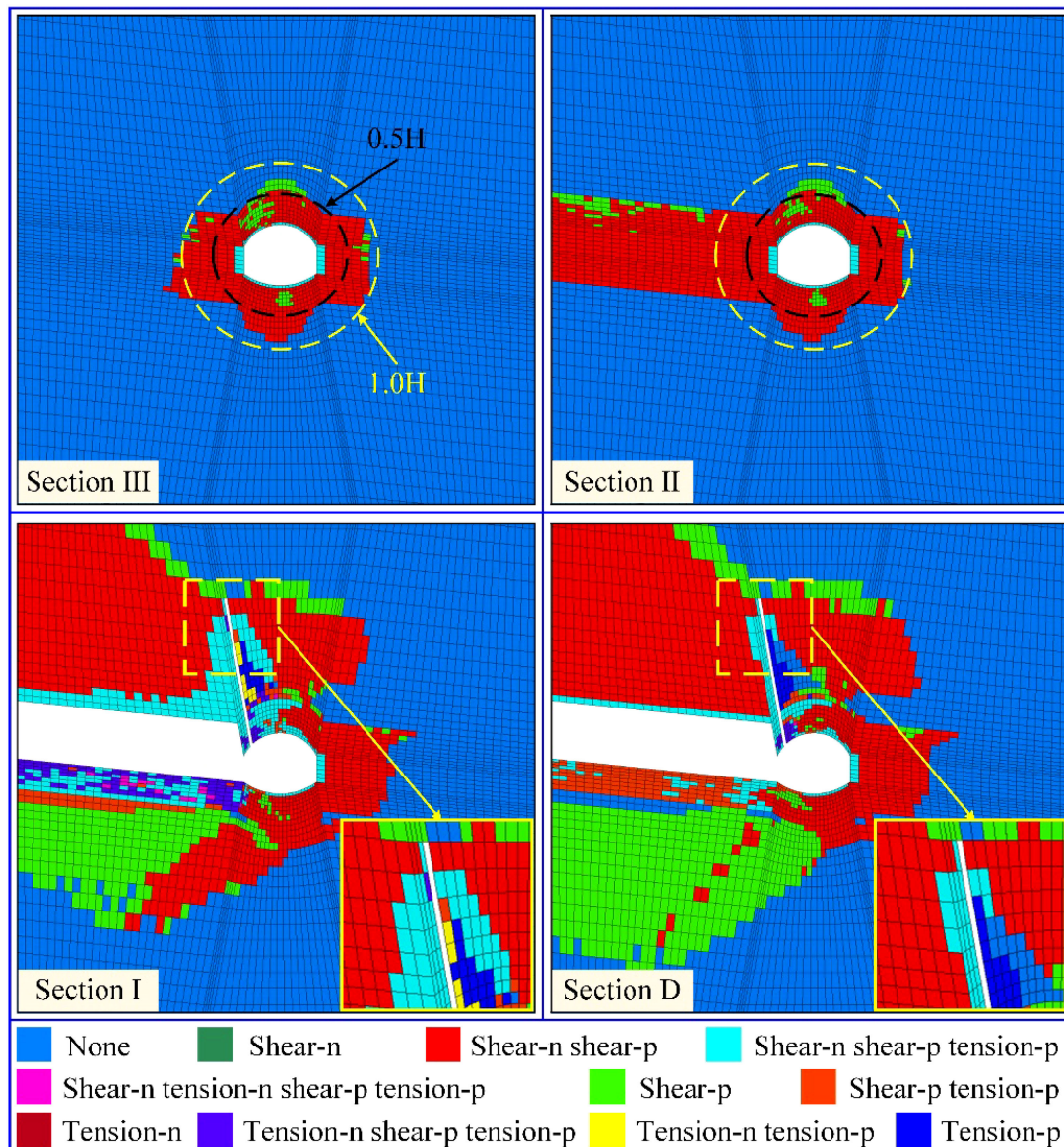


FIGURE 20 Characteristics of the distribution of the plastic zone.

The cut changes the stress distribution of the roadway. Except for the sidewall of the roadway, the average stress reduction of the surrounding rock is 16.7%. The average stress threshold at the transition between stage ④ and stage ⑤ is 1.29 MPa. If the stress exceeds 1.29 MPa, then the roadway is rapidly deformed, the stress is released rapidly, and the damage is irreversible. When the physical experiment results are converted on a similar scale, the corresponding stress threshold on site is 20.3 MPa. The numerical experiments show that the vertical stress in the main bearing area of the rock surrounding (within the range of 0.5H) the front roadway is less than 20.0 MPa. According to the Mohr–Coulomb criterion, the maximum principal stress in front of the roadway is reduced,

and the diameter of the stress circle shrinks to the strength envelope (Wang et al., 2022b), which can ensure the safety of the roadway, thereby reconciling the contradiction between the high stress and low carrying capacity of soft rocks (Zhan et al., 2022). The roof cutting reduces the average stress within the failure threshold, so the safety of the roadway can still be guaranteed without increasing the support.

6.3 Engineering recommendations

The following should be noted during the field implementation.

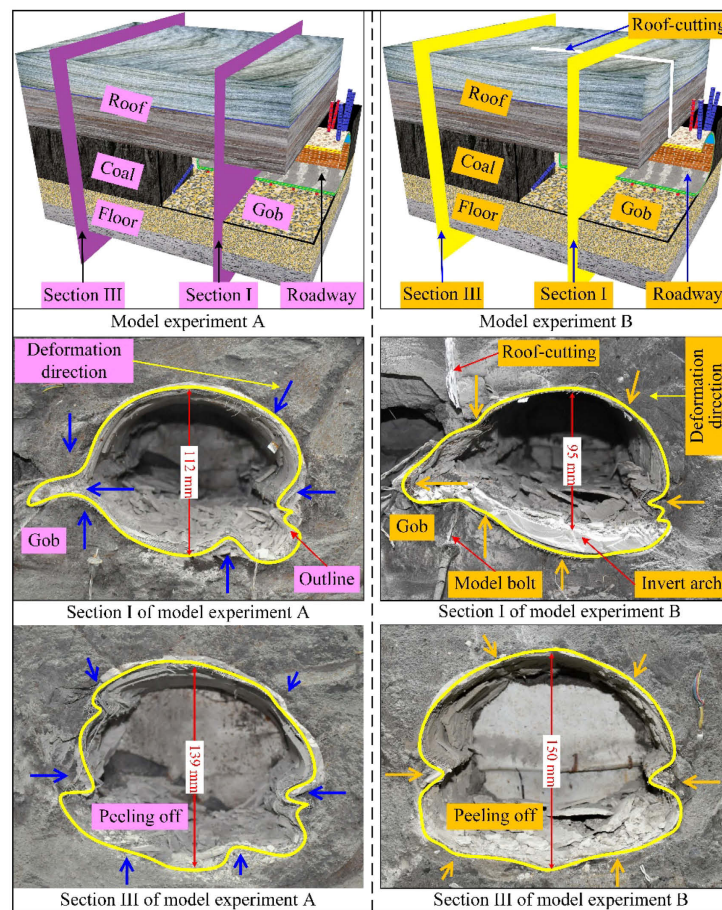


FIGURE 21
Failure characteristics of the two model experiments.

- (1) The metal mesh at the sidewall of the roadway can use sliding laps to increase the coordination of deformation.
- (2) The initial supporting force of the fully mechanized mining support should be improved, and the guard board should be used to prevent the coal from spalling in the longwall face.
- (3) The cable behind the longwall face should be unloaded in time to weaken the effect of the longitudinal connection of the roadway support.

7 Conclusions

Two 3D physical experiments were conducted to study the mechanism of roof cutting and pressure relief for roadway protection. The abutment stress, roadway convergence, and plastic area were investigated by numerical simulations. On the premise of not increasing the support strength of the roadway, roof cutting significantly improves the stability and safety of the soft-rock roadway. The following conclusions can be drawn.

- (1) Under mining influence, the soft-rock roadway is severely damaged, and the damage is closely related to the deformation of convergence. The roof cutting of the rear roadway effectively reduces the deformation of the front roadway. Specifically, the vertical deformation of the front roadway is reduced by 27.4%, and the coal pillar deformation is reduced by 15.7%.
- (2) The pattern of stress change at the 0.5H position of a coal mining roadway includes the growth stage, release stage and adjustment stage. The stress of the roadway near the roof cutting is significantly reduced. The stress on the roof in front of the longwall face is transferred to the panel to be mined, and the stress of the panel increases by 10%. The surrounding rock near the roof cutting exhibits obvious tensile–shear composite failure, and the plastic zone expands to the high position of the roof of the gob, which is more conducive to the deformation and collapse of the gob.
- (3) Roof cutting reduces the stress of the front roadway within the critical failure threshold, which fundamentally weakens the factors inducing roadway deformation and failure. On

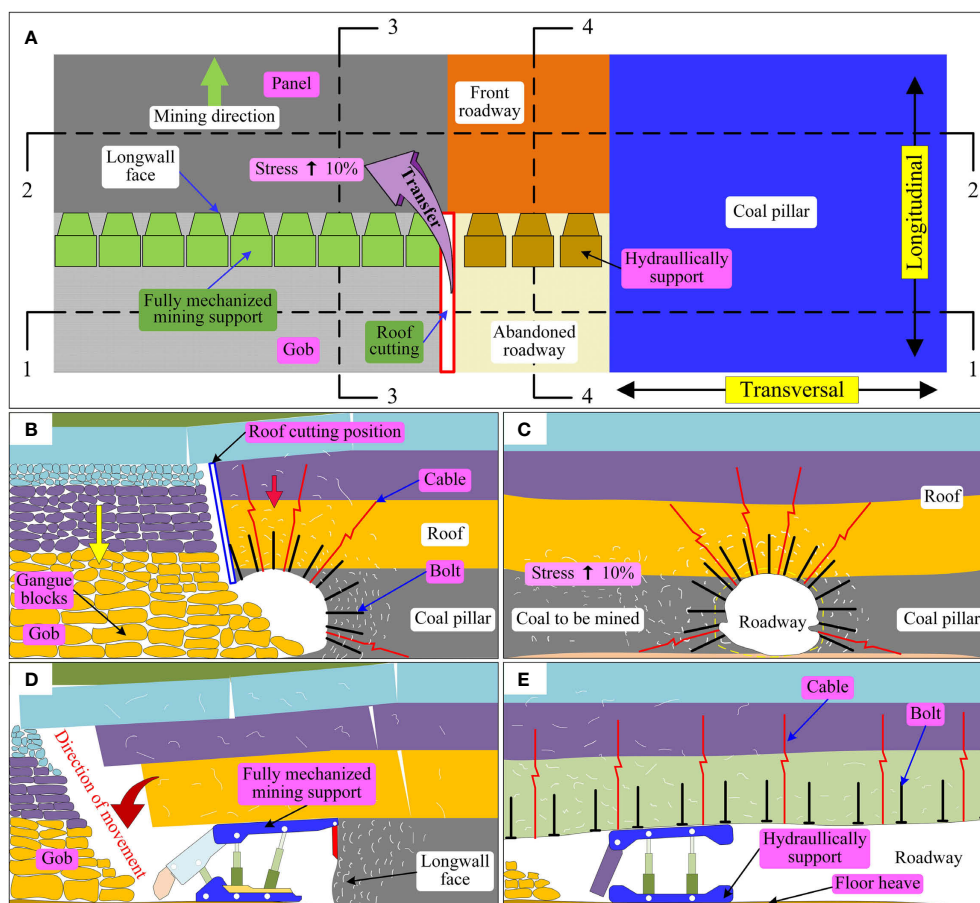


FIGURE 22 Characteristics of rock strata failure. (A) Four typical sections. (B) Section 1-1. (C) Section 2-2. (D) Section 3-3. (E) Section 4-4.

the premise of not increasing the support strength of the roadway, roof cutting significantly improves the stability and safety of the soft-rock roadway. This study can provide a reference for controlling the deformation of coal mining roadways.

Funding

This study was financially supported by the National Natural Science Foundation of China (No. 41772299).

Acknowledgments

The authors would like to thank the Shandong Key Laboratory of Civil Engineering Disaster Prevention and Mitigation (Shandong University of Science and Technology) and National Natural Science Foundation of China for their support. We sincerely thank the editor, associate editor and reviewers for their critical evaluation and constructive suggestions, which helped to improve the manuscript.

Data availability statement

The original contributions presented in the study are included in the article/supplementary material. Further inquiries can be directed to the corresponding author.

Author contributions

ZQ: formal analysis, investigation, visualization, writing, original draft. LT: conceptualization, funding acquisition, writing, methodology. LQ: validation, writing and editing. LY: software, formal analysis, data curation. LC: data curation, resources, investigation. CJ: resources, investigation. All authors have read and agreed to the published version of the manuscript.

Conflict of interest

CL and JC are employed by Inner Mongolia Shanghaimiao Mining Co., Ltd.

The remaining authors declare that the research was conducted in the absence of any commercial or financial relationships that could be construed as a potential conflict of interest.

Publisher's note

All claims expressed in this article are solely those of the authors and do not necessarily represent those of their affiliated

organizations, or those of the publisher, the editors and the reviewers. Any product that may be evaluated in this article, or claim that may be made by its manufacturer, is not guaranteed or endorsed by the publisher.

References

- Arora, K., Gutierrez, M., and Hedayat, A. (2022). Physical model simulation of rock-support interaction for the tunnel in squeezing ground. *J. Rock Mech. Geotech. Eng.* 14, 82–92. doi: 10.1016/j.jrmge.2021.08.016
- Arora, K., Gutierrez, M., Hedayat, A., and Xia, C. (2021). Tunnels in squeezing clay-rich rocks. *Undergr. Space* 6, 432–445. doi: 10.1016/j.undsp.2020.07.001
- Bian, W. H., Yang, J., He, M. C., Zhu, C., and Xu, D. M. (2022). Research and application of mechanical models for the whole process of 110 mining method roof structural movement. *J. Cent. South Univ.* 29, 3106–3124. doi: 10.1007/s11771-022-5148-9
- Castro, R., Trueman, R., and Halim, A. (2007). A study of isolated draw zones in block caving mines by means of a large 3D physical model. *Int. J. Rock Mech. Min. Sci.* 44, 860–870. doi: 10.1016/j.ijrmm.2007.01.001
- Chen, S. Y., Zhao, F., Wang, H. J., Yuan, G. X., Guo, Z. B., and Yang, J. (2019). Determination of key parameters of gob-side entry retaining by cutting roof and its application to a deep mine. *Rock Soil Mech.* 40, 332–342, 350. doi: 10.16285/j.rsm.2017.2194
- Fang, K., Tang, H. M., Li, C. D., Su, X. X., An, P. J., and Sun, S. X. (2023). Centrifuge modelling of landslides and landslide hazard mitigation: A review. *Geosci. Front.* 14, 101493. doi: 10.1016/j.gsf.2022.101493
- Ghabraie, B., Ren, G., Smith, J., and Holden, L. (2015). Application of 3D laser scanner, optical transducers and digital image processing techniques in physical modelling of mining-related strata movement. *Int. J. Rock Mech. Min. Sci.* 80, 219–230. doi: 10.1016/j.ijrmm.2015.09.025
- Guo, P. F., Yuan, Y. D., Ye, K. K., and Sun, D. J. (2021). Fracturing mechanisms and deformation characteristics of rock surrounding the gate during gob-side entry retention through roof pre-fracturing. *Int. J. Rock Mech. Min. Sci.* 148, 104927. doi: 10.1016/j.ijrmm.2021.104927
- Halder, P., and Manna, B. (2021). Large scale model testing to investigate the influence of granular cushion layer on the performance of disconnected piled raft system. *Acta Geotech.* 16, 1597–1614. doi: 10.1007/s11440-020-01121-5
- Hao, J., Li, X. L., Song, Y. C., Zhang, P. Z., and Liu, H. J. (2021). Analysis of mining roadway with large deformation of broken soft coal and research on supporting technology: A case study in Xin'an coal mine, China. *Eng. Fail. Anal.* 130, 105761. doi: 10.1016/j.engfailanal.2021.105761
- He, M. C., Ma, X. G., Yu, B., Stefano, S., and Sorace, S. (2019). Analysis of strata behavior process characteristics of gob-side entry retaining with roof cutting and pressure releasing based on composite roof structure. *Shock Vib.* 2019, 1–12. doi: 10.1155/2019/2380342
- He, F. L., Xu, X. H., Qin, B. B., Li, L., Lv, K., and Li, X. B. (2022). Study on deformation mechanism and control technology of surrounding rock during reuse of gob side entry retaining by roof pre-splitting. *Eng. Fail. Anal.* 137, 106271. doi: 10.1016/j.engfailanal.2022.106271
- Jongpradist, P., Tunsakul, J., Kongkitkul, W., Fadsiri, N., Arangelovski, G., and Youwai, S. (2015). High internal pressure induced fracture patterns in rock masses surrounding caverns: experimental study using physical model tests. *Eng. Geol.* 197, 158–171. doi: 10.1016/j.enggeo.2015.08.024
- Li, W. T., Li, X. M., Mei, Y. C., Wang, G., Yang, W. D., and Wang, H. T. (2022a). A numerical simulation approach of energy-absorbing anchor bolts for rock engineering. *Int. J. Rock Mech. Min. Sci.* 158, 105188. doi: 10.1016/j.ijrmm.2022.105188
- Li, H. B., Zhao, X. D., Dai, B. B., Huang, Z. J., and Zhu, Q. K. (2022b). Study on the evolution and prediction of fracture depth of surrounding rock in deep mining roadway based on numerical analysis and borehole detection. *Front. Earth Sci.* 10. doi: 10.3389/feart.2022.1024240
- Li, J., Lian, X. Y., Li, C., Wu, Z., and Wang, J. (2022c). Failure mechanism and support system of roofs in advance areas affected by mining under the condition of soft rock stratum. *Front. Earth Sci.* 10. doi: 10.3389/feart.2022.936029
- Lou, Q. N., Li, T. C., Zhu, Q. W., Wu, S. Y., Yun, M., and Zhao, R. L. (2021). A control approach of the roof in no-pillar roadway formed by roof cutting and pressure releasing. *Geofluids* 2021, 1–14. doi: 10.1155/2021/4303021
- Lv, H. Y., Cheng, Z. B., and Liu, F. (2021). Study on the mechanism of a new fully mechanical mining method for extremely thick coal seam. *Int. J. Rock Mech. Min. Sci.* 142, 104788. doi: 10.1016/j.ijrmm.2021.104788
- Mishra, S., Kumar, A., Rao, K. S., and Gupta, N. K. (2021). Experimental and numerical investigation of the dynamic response of tunnel in soft rocks. *Structures* 29, 2162–2173. doi: 10.1016/j.istruc.2020.08.055
- Mo, S., Ramandi, H. L., Oh, J., Masoumi, H., Canbulat, I., Hebblewhite, B., et al. (2020). A new coal mine floor rating system and its application to assess the potential of floor heave. *Int. J. Rock Mech. Min. Sci.* 128, 104241. doi: 10.1016/j.ijrmm.2020.104241
- Najm, S. J., and Daraei, A. (2023). Forecasting and controlling two main failure mechanisms in the Middle East's longest highway tunnel. *Eng. Fail. Anal.* 146, 107091. doi: 10.1016/j.engfailanal.2023.107091
- Öge, İ. F. (2021). Revisiting the assessment of squeezing condition and energy absorption of flexible supports: A mine development case. *Tunn. Undergr. Space Technol.* 108, 103712. doi: 10.1016/j.tust.2020.103712
- Pan, R., Wang, Q., Jiang, B., Li, S. C., Sun, H. B., Qin, Q., et al. (2017). Failure of bolt support and experimental study on the parameters of bolt-grouting for supporting the roadways in deep coal seam. *Eng. Fail. Anal.* 80, 218–233. doi: 10.1016/j.engfailanal.2017.06.025
- Shen, B. T. (2014). Coal mine roadway stability in soft rock: a case study. *Rock Mech. Rock Eng.* 47, 2225–2238. doi: 10.1007/s00603-013-0528-y
- Shimamoto, K., and Yashiro, K. (2021). New rockbolting methods for reinforcing tunnels against deformation. *Int. J. Rock Mech. Min. Sci.* 147, 104898. doi: 10.1016/j.ijrmm.2021.104898
- Sun, Y. T., Bi, R. Y., Sun, J. B., Zhang, J. F., Taherdangkoo, R., Huang, J. D., et al. (2022). Stability of roadway along hard roof goaf by stress relief technique in deep mines: a theoretical, numerical and field study. *Geomech. Geophys. Geo-Energy Resour.* 8, 1–16. doi: 10.1007/s40948-022-00356-8
- Tian, M. L., Han, L. J., Xiao, H. T., and Meng, Q. B. (2021). Experimental study of deformations and failures of the coal wall in a longwall working face. *Eng. Fail. Anal.* 125, 105428. doi: 10.1016/j.engfailanal.2021.105428
- Tian, M. L., Han, L. J., Yang, X. X., Feng, Q., Meng, Q. B., Xie, Y. Y., et al. (2022). Asymmetric deformation failure mechanism and support technology of roadways under non-uniform pressure from a mining disturbance. *Bull. Eng. Geol. Environ.* 81, 1–14. doi: 10.1007/s10064-022-02710-2
- Wang, X. Q., Li, Y. M., Zhao, C. X., Wang, Y., and Huang, S. J. (2021). Study on deformation failure mechanism and control technology of surrounding rock in soft rock roadway. *Geotech. Geol. Eng.* 39, 5931–5942. doi: 10.1007/s10706-021-01977-8
- Wang, Q., Jiang, B., Xu, S., He, M. C., Jiang, Z. H., Li, S. C., et al. (2022a). Roof-cutting and energy-absorbing method for dynamic disaster control in deep coal mine. *Int. J. Rock Mech. Min. Sci.* 158, 105186. doi: 10.1016/j.ijrmm.2022.105186
- Wang, Y. J., Wang, Q., Tian, X. C., Wang, H. S., Yang, J., and He, M. C. (2022b). Stress and deformation evolution characteristics of gob-side entry retained by roof cutting and pressure relief. *Tunn. Undergr. Space Technol.* 123, 104419. doi: 10.1016/j.tust.2022.104419
- Xu, X. H., He, F. L., Li, X. B., and He, W. R. (2021). Research on mechanism and control of asymmetric deformation of gob side coal roadway with fully mechanized caving mining. *Eng. Fail. Anal.* 120, 105097. doi: 10.1016/j.engfailanal.2020.105097
- Xue, T. E., Zhang, Q. Y., Duan, K., Wang, P. F., Lin, H. X., Fan, Q. H., et al. (2022). Geo-mechanical model test on the water inrush induced by zonal disintegration of deep tunnel under hydro-mechanical coupling. *Int. J. Rock Mech. Min. Sci.* 160, 105278. doi: 10.1016/j.ijrmm.2022.105278
- Yang, S. Q., Chen, M., Jing, H. W., Chen, K. F., and Meng, B. (2017). A case study on large deformation failure mechanism of deep soft coal roadway in Xin'an coal mine, China. *Eng. Geol.* 217, 89–101. doi: 10.1016/j.enggeo.2016.12.012
- Yang, X. J., Hu, C. W., He, M. C., Wang, H. H., Zhou, Y. B., Liu, X. Y., et al. (2019). Study on presplitting blasting the roof strata of adjacent roadway to control roadway deformation. *Shock Vib.* 2019, 1–16. doi: 10.1155/2019/3174898
- Yang, X. J., Huang, R. F., Yang, G., Wang, Y. J., Cao, J. D., Liu, J. N., et al. (2021). Validation study of no-pillar mining method without advance tunneling: A case study of a mine in China. *Energy Sci. Eng.* 9, 1761–1772. doi: 10.1002/ese3.949
- Zhan, Q. J., Muhammad Shahani, N., Zheng, X. G., Xue, Z. C., and He, Y. Y. (2022). Instability mechanism and coupling support technology of full section strong convergence roadway with a depth of 1350 m. *Eng. Fail. Anal.* 139, 106374. doi: 10.1016/j.engfailanal.2022.106374
- Zhan, Q. J., Zheng, X. G., Du, J. P., and Xiao, T. (2020). Coupling instability mechanism and joint control technology of soft-rock roadway with a buried depth of 1336 m. *Rock Mech. Rock Eng.* 53, 2233–2248. doi: 10.1007/s00603-019-02027-9
- Zhang, Q., He, M. C., Guo, S., Qi, J. C., Yang, J., Wang, C., et al. (2022). Investigation on the key techniques and application of the new-generation automatically formed roadway without coal pillars by roof cutting. *Int. J. Rock Mech. Min. Sci.* 152, 105058. doi: 10.1016/j.ijrmm.2022.105058
- Zhang, L. B., Shen, W. L., Li, X. L., Wang, Y. B., Qin, Q. Z., Lu, X. T., et al. (2023). Abutment pressure distribution law and support analysis of super large mining height face. *Int. J. Environ. Res. Public Health* 20, 227. doi: 10.3390/ijerph20010227

- Zhang, C., Wang, F. T., and Bai, Q. S. (2021). Underground space utilization of coalmines in China: A review of underground water reservoir construction. *Tunn. Undergr. Space Technol.* 107, 103657. doi: 10.1016/j.tust.2020.103657
- Zheng, H. B., Li, P. F., and Ma, G. W. (2021). Stability analysis of the middle soil pillar for asymmetric parallel tunnels by using model testing and numerical simulations. *Tunn. Undergr. Space Technol.* 108, 103686. doi: 10.1016/j.tust.2020.103686
- Zhou, H., Zhang, C., Li, Z., Hu, D., and Hou, J. (2014). Analysis of mechanical behavior of soft rocks and stability control in deep tunnels. *J. Rock Mech. Geotech. Eng.* 6, 219–226. doi: 10.1016/j.jrmge.2014.03.003
- Zhu, Z. G., Fang, Z. C., Xu, F., Han, Z. M., Guo, X. L., and Ma, C. Y. (2022c). Model test study on the rock mass deformation law of a soft rock tunnel under different ground stresses. *Front. Earth Sci.* 10. doi: 10.3389/feart.2022.962445
- Zhu, Q. W., Li, T. C., Du, Y. T., Zhang, H., Ran, J. L., Li, W. T., et al. (2022a). Failure and stability analysis of deep soft rock roadways based on true triaxial geomechanical model tests. *Eng. Fail. Anal.* 137, 106255. doi: 10.1016/j.engfailanal.2022.106255
- Zhu, Q. W., Li, T. C., Wang, B. X., Li, C. J., Ran, J. L., and Zhang, H. (2023). A case study on the deformation and failure mechanism of a soft rock mining roadway in the Xin'Shang'Hai No. 1 coal mine, China. *Eng. Fail. Anal.* 146, 107136. doi: 10.1016/j.engfailanal.2023.107136
- Zhu, Q. W., Li, T. C., Zhang, H., Ran, J. L., Li, H., Du, Y. T., et al. (2022b). True 3D geomechanical model test for research on rheological deformation and failure characteristics of deep soft rock roadways. *Tunn. Undergr. Space Technol.* 128, 104653. doi: 10.1016/j.tust.2022.104653